

Antigen-presenting innate lymphoid cells orchestrate neuroinflammation

<https://doi.org/10.1038/s41586-021-04136-4>

Received: 11 October 2019

Accepted: 14 October 2021

Published online: 1 December 2021

 Check for updates

John B. Grigg^{1,2,3}, Arthi Shanmugavadivu^{4,9}, Tommy Regen^{4,9}, Christopher N. Parkhurst^{1,2,3}, Anees Ahmed^{1,2,3}, Ann M. Joseph^{1,2,3}, Michael Mazzucco⁵, Konrad Gronke^{6,7}, Andreas Diefenbach^{6,7}, Gerard Eberl⁸, Timothy Vartanian⁵, Ari Waisman^{4,10} & Gregory F. Sonnenberg^{1,2,3,10}✉

Pro-inflammatory T cells in the central nervous system (CNS) are causally associated with multiple demyelinating and neurodegenerative diseases^{1–6}, but the pathways that control these responses remain unclear. Here we define a population of inflammatory group 3 innate lymphoid cells (ILC3s) that infiltrate the CNS in a mouse model of multiple sclerosis. These ILC3s are derived from the circulation, localize in proximity to infiltrating T cells in the CNS, function as antigen-presenting cells that restimulate myelin-specific T cells, and are increased in individuals with multiple sclerosis. Notably, antigen presentation by inflammatory ILC3s is required to promote T cell responses in the CNS and the development of multiple-sclerosis-like disease in mouse models. By contrast, conventional and tissue-resident ILC3s in the periphery do not appear to contribute to disease induction, but instead limit autoimmune T cell responses and prevent multiple-sclerosis-like disease when experimentally targeted to present myelin antigen. Collectively, our data define a population of inflammatory ILC3s that is essential for directly promoting T-cell-dependent neuroinflammation in the CNS and reveal the potential of harnessing peripheral tissue-resident ILC3s for the prevention of autoimmune disease.

Multiple sclerosis (MS) is an autoimmune disease driven by pro-inflammatory T cells that are reactive to self-antigens in the CNS^{1,2}. Emerging data indicate that similar pathways drive neurodegenerative diseases, including Alzheimer's disease^{3,4} and Parkinson's disease^{5,6}. Genetic associations with major histocompatibility complex class II (MHCII) have been identified in patient cohorts^{7–10} and antigen-specific CD4 T cells contribute to disease pathogenesis in mouse models^{11–15}. Despite these advances, the mechanisms that regulate pro-inflammatory T cells in the CNS are incompletely understood.

Unique ILC3s infiltrate the inflamed CNS

ILC3s resemble activated T cells, have dynamic interactions with adaptive immunity^{16,17} and can associate with the meninges or CNS^{18–20}. To better understand ILC3s in the context of autoimmune neuroinflammation, we induced active experimental autoimmune encephalomyelitis (EAE), a mouse model of MS, in mice reporting eGFP under control of the ROR γ t promoter (Rorc-eGFP). From disease onset through chronic phases of EAE, we observed significantly increased frequencies and numbers of ILC3s in the CNS, dura meninges and cervical lymph nodes relative to naive mice (Fig. 1a, b, Extended Data Fig. 1a, b). ILC3s

comprised approximately 22% of the total ROR γ t⁺ population within the CNS (Extended Data Fig. 1c), were increased in wild-type mice (Extended Data Fig. 1d) and required antigen-dependent induction of neuroinflammation (Extended Data Fig. 1e). ILC3s also increased in the immunization-draining inguinal lymph nodes and cervical lymph nodes during the peak of EAE; however, this occurred independently of EAE (Extended Data Fig. 1e).

ILC3s exhibit considerable heterogeneity and plasticity¹⁶. To investigate this in neuroinflammation, we induced EAE in mice that fate-map ROR γ t expression with the yellow fluorescent protein gene (eYFP). We found that a majority of eYFP-marked ILC3s in the CNS co-stained for ROR γ t protein, whereas by comparison, a greater proportion of eYFP⁺ ILC3s in the mesenteric lymph node downregulated ROR γ t protein (Fig. 1c, Extended Data Fig. 1f), showing that ILC3s in the inflamed CNS stably express ROR γ t. In agreement with this, the eYFP⁺ ILC3 population in the CNS was predominantly CCR6⁺ and Nkp46[–] relative to more-heterogeneous populations in the small intestine lamina propria (Fig. 1d), and expressed moderate levels of T-bet, but did not convert to an 'ex-ILC3' Nkp46⁺T-bet⁺ population (Extended Data Fig. 1g). By comparison, a previously described²⁰ Nkp46⁺T-bet⁺ ILC1-like population could be detected within the YFP[–] lymphoid fraction during EAE (Extended Data Fig. 1g), indicating that ILC1s and ILC3s in the CNS are

¹Jill Roberts Institute for Research in Inflammatory Bowel Disease, Weill Cornell Medicine, Cornell University, New York, NY, USA. ²Joan and Sanford I. Weill Department of Medicine, Weill Cornell Medicine, Cornell University, New York, NY, USA. ³Department of Microbiology and Immunology, Weill Cornell Medicine, Cornell University, New York, NY, USA. ⁴Institute for Molecular Medicine, University Medical Center of the Johannes Gutenberg University Mainz, Mainz, Germany. ⁵Brain and Mind Research Institute, Weill Cornell Medicine, Cornell University, New York, NY, USA. ⁶Laboratory of Innate Immunity, Department of Microbiology, Infectious Diseases and Immunology, Charité—Universitätsmedizin Berlin, Berlin, Germany. ⁷Mucosal and Developmental Immunology, Deutsches Rheuma-Forschungszentrum (DRFZ), Berlin, Germany. ⁸Microenvironment and Immunity Unit, Institut Pasteur, Paris, France. ⁹These authors contributed equally: Arthi Shanmugavadivu, Tommy Regen. ¹⁰These authors jointly supervised this work: Ari Waisman, Gregory F. Sonnenberg. ✉e-mail: gfsonnenberg@med.cornell.edu

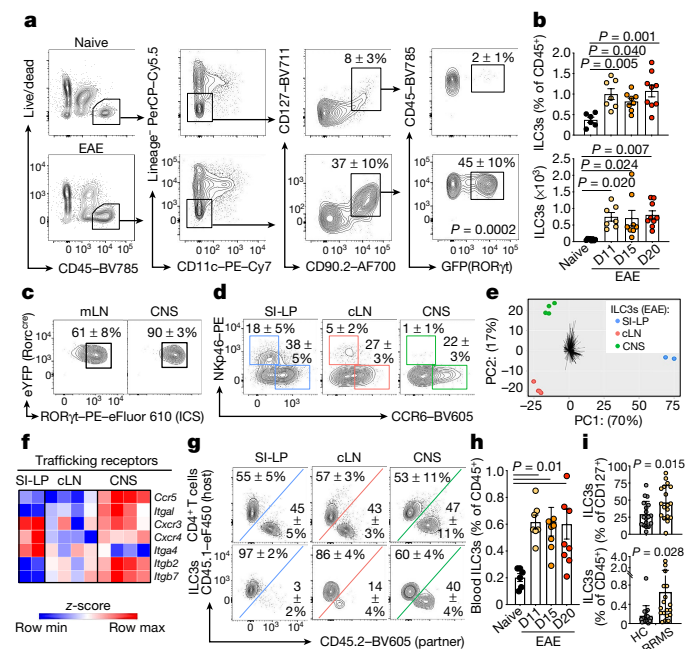


Fig. 1 | A unique subset of ILC3s infiltrates the CNS during neuroinflammation. **a, b,** Representative flow cytometry for ILC3s (**a**; $n = 4$ mice per group) and quantification of total frequency and cell counts (**b**) in the CNS (brain and spinal cord) of Rorc-eGFP mice at steady state (naive) ($n = 6$ mice) versus EAE onset (day (D) 11, $n = 7$), acute (D15, $n = 8$) or chronic (D20, $n = 9$) phase. Lineage: CD3 ϵ , CD5, CD8 α , TCR $\gamma\delta$, NK1.1, CD11b, B220, Ly6C. **c, d,** Representative intracellular staining (ICS) of ROR γ t (c) or ILC3 heterogeneity (d) on eYFP⁺ ILCs in Rorc-cre^{eYFP} mice at day 15 EAE ($n = 4$ mice). cLN, cervical lymph nodes; mLN, mesenteric lymph nodes; SI-LP, small intestine lamina propria. **e,** Principal component analysis of gene expression from RNA sequencing of flow-sorted ILC3s from Rorc-eGFP mice ($n = 4$ mice). **f,** Heat map showing relative expression z-scores of the indicated genes in sorted ILC3s. **g,** Representative flow cytometry showing chimerism of host (CD45.1⁻) versus partner (CD45.2⁺) derived CD4 T cells or ILC3s during EAE ($n = 4$ mice per tissue). **h,** Frequency of ILC3s in the blood of Rorc-eGFP mice during EAE. **i,** Frequency of ILC3s in peripheral blood mononuclear cells (PBMCs) of patients with relapsing-remitting multiple sclerosis (RRMS) versus age- and sex-matched healthy control individuals (HC) ($n = 18$ samples per group). Data in **a, c, d, g** are representative of three independent experiments with similar results. Data in **b, h** are pooled from two independent experiments with similar results. Mean \pm s.d. Statistics calculated by unpaired, two-tailed *t*-test (Mann-Whitney *U*-test) (**a**), one-way ANOVA with Sidak's multiple comparisons test (**b, h**), or two-tailed, paired *t*-test (**i**).

independent populations. We next performed RNA sequencing on sort-purified ILC3s from various tissues during EAE and observed significant differences in the global transcriptional signatures (Fig. 1e). All sorted populations expressed classical ILC3-associated transcriptional signatures and low levels of other immune-cell-lineage-specific genes (Extended Data Fig. 2a). We also did not detect the expression of *Aire* in ILC3s in any tissue, indicating that they are distinct from extra-thymic AIRE-expressing cells in the periphery²¹. Furthermore, CNS-associated ILC3s exhibited unique markers of ILC3 heterogeneity relative to well-described ILC3 subsets in the intestine or lymph node, including high expression of T-bet (but not Nkp46), CCR6 (but not CD4), IFN γ and TNF (Fig. 1d, Extended Data Figs. 1c, g, 2b–d).

ILC3s in the intestine and peripheral lymph nodes are seeded early during development and remain tissue-resident, even during inflammation²². However, the presence and phenotype of ILC3s in the CNS during EAE prompted us to investigate their ontogeny. We identified that ILC3s in the CNS uniquely expressed trafficking receptors *Ccr5*, *Itgal*, *Itgb2* and *Itgb7* (Fig. 1f) that are critical for the entry of lymphocytes into the inflamed CNS through the circulation²³.

To examine this further, we joined the circulation of congenic mice through parabiosis and induced EAE. At disease onset, we observed that nearly all ILC3s in the small intestine lamina propria and cervical lymph nodes remained of host origin, whereas those in the CNS exhibited mixed origins from both the host and the parabiotic partner mouse (Fig. 1g), showing that ILC3s in the CNS uniquely derive from the circulation. By comparison, CD4 T cells in all tissues were of mixed host origin (Fig. 1g), confirming efficient blood chimerism. We also observed significantly increased numbers of ILC3-like cells in the circulation during EAE relative to naive mice (Fig. 1h), and significantly increased frequencies of ROR γ t⁺ ILC3-like cells in the blood of patients with MS relative to age- and sex-matched control individuals (Fig. 1i, Extended Data Fig. 2e, Supplementary Table 1). This is consistent with previous reports of ILC3-like cells in patients with MS^{24–27}. Collectively, these data define a subset of ILC3s during neuroinflammation that migrate from the circulation to the CNS, are increased in the blood of mice and humans and exhibit a unique pro-inflammatory phenotype.

ILC3s present antigen in the inflamed CNS

ILC3s directly modulate adaptive immunity through antigen presentation and MHCII^{28–30}. Analyses of ILC3s in the cervical lymph nodes and CNS during EAE revealed high expression levels of *H2-Ab1*, *H2-Aa* and *Cd74* (Fig. 2a). With the induction of EAE, ILC3s in the CNS upregulate MHCII and increase in frequency, and this was dependent on neuroinflammation (Fig. 2b, c, Extended Data Fig. 3a, b). By contrast, ILC3s in the blood of mice and humans (Extended Data Fig. 3a, c) do not express MHCII. CNS-associated ILC3s uniquely express higher levels of gene transcripts for the canonical pathway of IFN γ -mediated induction of MHCII^{31,32} and several cathepsins³³ (Fig. 2d). We previously showed that MHCII⁺ ILC3s in the intestine lack conventional co-stimulatory molecules and promote T cell tolerance to the microbiota^{28,29}, whereas others have reported that splenic ILC3-like cells upregulate canonical co-stimulatory molecules and promote T cell responses after vaccination³⁰. We observe that CNS-associated ILC3s exhibit numerous co-stimulatory molecules, T-cell-activating cytokines and other inflammatory mediators that have previously been implicated in the pathogenesis of EAE^{34–37} (Fig. 2d). This includes CD80 and CD86, which are absent on circulating ILC3-like cells and tissue-resident ILC3s in the inguinal, cervical and mesenteric lymph nodes, but are found on CNS-associated ILC3s during EAE (Extended Data Figs. 3d, e, 4a). ILC3s in the CNS and lymph nodes did not express CD40, CD30L or OX40L (Extended Data Fig. 4b). We also detected ILC3s in the cerebral spinal fluid (CSF) of patients with MS and we observed that among these patients, the frequency of ILC3s positively trended with the presence of contrast-enhancing lesions (Extended Data Fig. 5a–d, Supplementary Table 2) and the ILC3s expressed MHCII (HLA-DR) and CD86 (Extended Data Fig. 5e). These results suggest that tissue-resident ILC3s in the periphery maintain a tolerogenic phenotype during EAE, whereas circulation-derived ILC3s mature to express MHCII, co-stimulatory molecules and other pathways that promote T cell activation in the inflamed CNS.

The pathogenic activity of encephalitogenic T cells is dependent on local reactivation by MHCII⁺ myeloid cells in the CNS. This process depends on perivascular-associated conventional dendritic cells (cDCs) that stimulate T cells during EAE^{38,39}. However, whether there are additional non-redundant MHCII⁺ cells that restimulate T cells in the parenchyma or myelin-rich white matter of the CNS is still an active area of investigation^{40,41}. We hypothesized that ILC3s have the potential to reactivate and provoke CD4 T cell responses in the CNS. In support of this hypothesis, we found that ILC3s in the brain and spinal cord were enriched predominantly within focal lesions of the CNS parenchyma, including the myelin-rich brainstem, spinal cord and cerebellum during EAE, and localized in direct proximity with infiltrating T cells

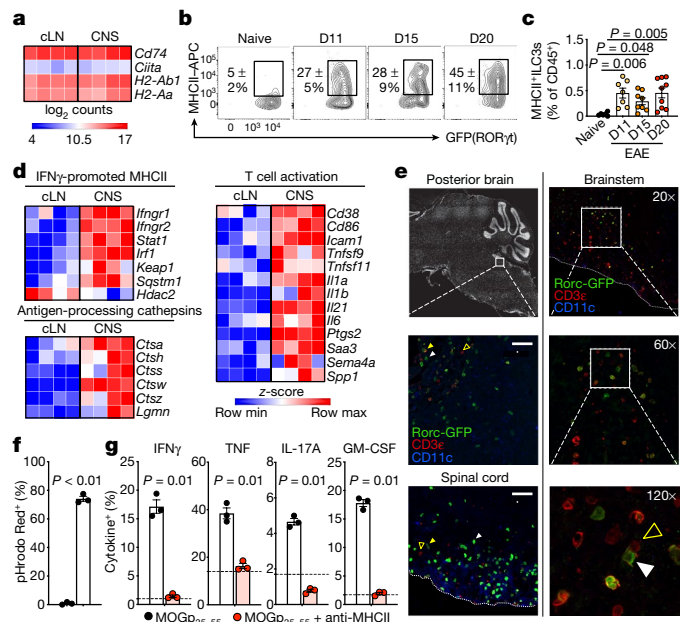


Fig. 2 | CNS-associated ILC3s restimulate encephalitogenic T cells in the CNS.

a, d, Heat maps showing absolute log-normalized counts ($\log_2(\text{count} + 1)$) (**a**) or relative expression z-scores (**d**) from RNA sequencing of the indicated genes in sorted ILC3s from Rorc-eGFP mice during the peak of active EAE ($n = 4$ mice). **b, c,** Representative flow cytometry (**b**) and frequency quantification (**c**) of MHCII⁺ ILC3s in the CNS (brain and spinal cord) of Rorc-eGFP mice at steady state (naive) ($n = 6$ mice) versus EAE onset (D11, $n = 7$), acute (D15, $n = 8$) or chronic (D20, $n = 9$) phase. **e,** Representative immunofluorescence staining of fixed brain, spinal cord and brainstem from Rorc-eGFP mice at day 18 of active EAE showing proximity (left) and example of co-localization (right), with increasing magnification between ILC3s (DAPI⁺CD11c⁺CD3⁺GFP⁺) and T cells (DAPI⁺CD11c⁺CD3⁺GFP⁺) in focal lesions. Representative ILC3s are indicated with white arrows, GFP⁺ T cells with yellow arrows and GFP⁻ T cells with unfilled yellow arrows. Spinal cord and brainstem borders are denoted with a fine-dashed white line. Scale bars, 50 μm . **f, g,** ILC3s and myelin-specific T cells were sorted from the CNS (day 19 EAE, pooled from $n = 8$ mice). **f,** ILC3s alone were incubated with pHrodo Red-labelled myelin-basic protein for two hours at the indicated temperatures and the frequency of pHrodo Red⁺ ILC3s was quantified by flow cytometry. **g,** ILC3s and myelin-specific T cells were co-cultured in the presence of peptide (MOGp) and anti-MHCII blocking antibody, and the frequency of cytokine-producing T cells was quantified by flow cytometry. Data points indicate technical well replicates and dashed lines indicate baseline cytokine production by T cells alone in the presence of peptide. Data in **c** are pooled from two independent experiments and data are representative of two (**b, e**) or three (**f, g**) independent experiments with similar results. Mean \pm s.d. Statistics calculated by one-way ANOVA with Sidak's multiple comparisons test (**c, g**) or unpaired, two-tailed *t*-test (Mann-Whitney *U*-test) (**f**).

(Fig. 2e, Extended Data Fig. 6a). By contrast, CD11c⁺ cDCs were mostly concentrated at the border-associated brain dura meninges and spinal cord leptomeninges (Fig. 2e, Extended Data Fig. 6a), as previously reported³⁹. Furthermore, sort-purified ILC3s from the CNS during EAE could take up pHrodo Red-labelled myelin basic protein (Fig. 2f), and co-culture could promote antigen- and MHCII-dependent production of the pro-inflammatory cytokines IFN γ , TNF, IL-17A and GM-CSF by myelin-specific T cells from the CNS (Fig. 2g). This was comparable to co-culture with sort-purified cDCs (Extended Data Fig. 6b, c), although it is possible that cytokine production reflects the induction of energy in this *in vitro* system. ILC3s also processed and presented full-length recombinant protein to reactivate and expand myelin-specific T cells in an MHCII-dependent manner (Extended Data Fig. 6d). Collectively, these data show that ILC3s are a bona fide antigen-presenting cell in the CNS parenchyma during autoimmune neuroinflammation.

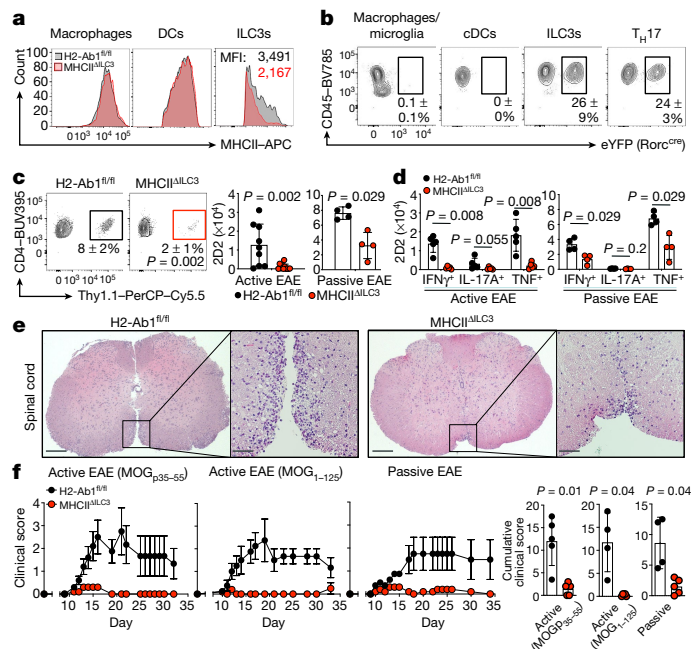


Fig. 3 | MHCII⁺ ILC3s in the CNS promote autoimmune T cells and demyelinating disease.

a, Representative flow cytometry histograms showing MHCII gated on the indicated cell subsets: macrophages (CD45⁺Ly6C⁻Ly6G⁺F4/80⁺CD64⁺), dendritic cells (DCs) (CD45⁺Ly6G⁻Ly6C⁺F4/80⁺CD64⁺CD11c⁺) or ILC3s (CD45⁺lineage⁻CD127⁺CD90.2⁺ROR γ t⁺) analysed from the cervical lymph nodes of either H2-Ab1^{fl/fl} or MHCII^{ΔILC3} mice at steady state; the geometric mean fluorescence intensity (MFI) is shown for ILC3s ($n = 4$ mice per group). **b,** Representative flow cytometry of eYFP expression from the indicated cell populations of Rorc-cre^{eYFP} mice in the CNS at day 15 EAE ($n = 6$ mice). **c–f,** Naive myelin-specific T cells (Thy1.1⁺) were transferred into recipient mice, which were then immunized 24 h later to induce active EAE ($n = 9$ or 11 mice per group), or EAE was induced by passive transfer of activated myelin-specific T cells ($n = 4$ mice per group). **c, d,** At day 15 after immunization or day 18 after passive transfer, donor T cells were analysed by flow cytometry for frequency and counts (**c**) and absolute counts of cytokine-producing donor T cells (**d**) in the CNS were quantified by flow cytometry ($n = 4$ or 5 mice per group). **e,** Representative haematoxylin and eosin (H&E) staining of fixed transverse spinal cord sections of mice shown at 4 \times magnification (left; scale bars, 300 μm) with 20 \times inset magnification (right; scale bars, 75 μm) of ventromedial fissure ($n = 5$ mice per group) at day 15 of active EAE. **f,** Average daily disease clinical scores of mice after induction of active or passive models of EAE, and cumulative clinical scores up to day 20 ($n = 4$ or 5 mice per group). Data are representative of two (**a, b**) or three (**c–f**) independent experiments with similar results. Data in **c** are pooled from two independent experiments. Mean \pm s.d. (**a–d**, f right three panels) or s.e.m. (f left three panels). Statistics calculated by unpaired, two-tailed *t*-test (Mann-Whitney *U*-test) (**c, f**) or two-way ANOVA with Sidak's multiple comparisons test (**d**).

MHCII⁺ ILC3s promote CNS inflammation

To test the functional importance of antigen-presenting ILC3s in the CNS, we used H2-Ab1-floxed mice crossed with Rorc^{cre} mice (MHCII^{ΔILC3} mice^{28,29}) and observed a specific loss of MHCII on ILC3s, but no effect of MHCII levels on macrophages, microglia, cDC subsets or monocytes in both the lymph nodes and the CNS relative to littermate controls (Fig. 3a, Extended Data Fig. 7a). We also induced EAE in mice that fate-map ROR γ t expression as above, measured for eYFP within lymphocytes and all major myeloid populations (Extended Data Fig. 7b) in the CNS and periphery, and were only able to detect eYFP amongst lymphocytes (Fig. 3b, Extended Data Fig. 7c) dominantly composed of CD4 T cells and ILC3s (Fig. 3b, Extended Data Fig. 7d). Next, we induced active EAE in MHCII^{ΔILC3} mice and littermate controls in conjunction with a pre-transfer of naive, myelin-specific T cells to permit *in vivo*

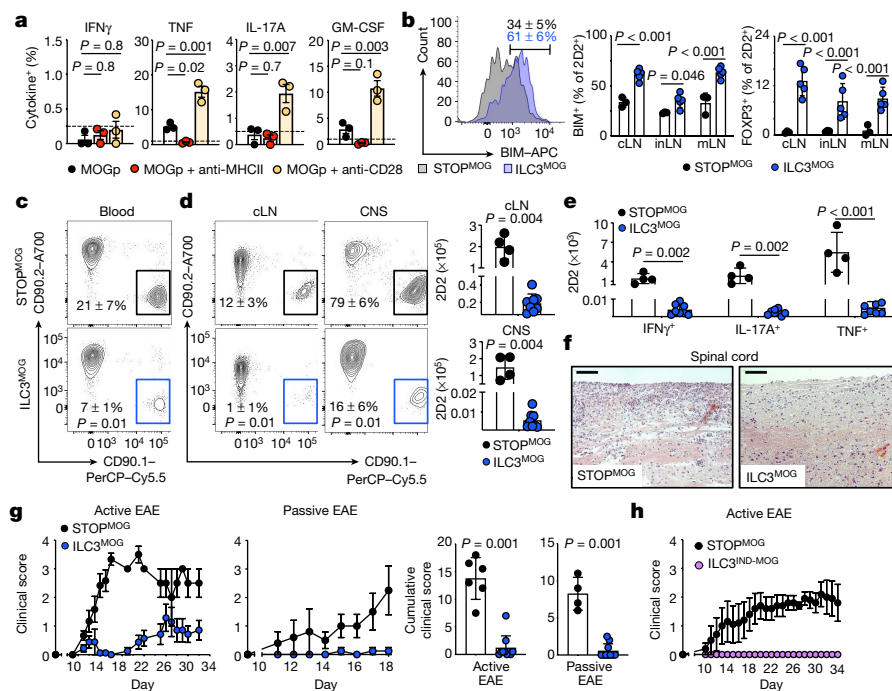


Fig. 4 | Peripheral tissue-resident ILC3s can be harnessed to prevent neuroinflammation. **a**, Frequency of cytokine⁺ myelin-specific T cells after 72 h co-culture with ex vivo-sorted ILC3s from the mesenteric lymph nodes (day 19 EAE, pooled from $n = 8$ mice) in the presence of antigen (MOGp) with or without anti-MHCII blocking antibody or anti-CD28 cross-linking antibody. Data points indicate technical well replicates and dashed lines indicate baseline cytokine production by T cells alone (sorted from mesenteric lymph nodes) in the presence of antigen alone. **b**, Naive myelin-specific T cells were transferred into recipient mice, which were then immunized 24 h later to induce active EAE. At day 7 after immunization, donor T cells were analysed by flow cytometry for the frequency of BIM⁺ or FOXP3⁺ ($n = 3$ or 5 mice per group). **c–f**, In vitro-activated Thy1.1⁺ myelin-specific T cells were transferred into recipient mice and the circulating frequency of transferred T cells was quantified by flow cytometry 8 days after transfer ($n = 5$ or 8 mice per group)

(c). At day 16, frequencies and absolute counts of donor T cells were quantified in the cervical lymph nodes and CNS (d) and counts of cytokine producing donor T cells in the CNS were quantified by flow cytometry (e). f, Representative H&E of fixed longitudinal spinal cord sections of mice at day 18 of passive EAE shown at 20 \times magnification. Scale bars, 100 μ m. g, Average daily disease clinical scores of mice after induction of active ($n = 6$ or 8 mice) or passive EAE ($n = 4$ or 8 mice) and cumulative clinical scores up to day 20 (each representative of 3 independent experiments). h, Average daily disease clinical scores of mice after treatment with tamoxifen 4 weeks before the induction of active EAE ($n = 4$ or 5 mice per group). Data in a–h are representative of two (b, h) or three (a, c–f, g) independent experiments with similar results. Mean \pm s.d. (a–e, g right two panels) or s.e.m. (g left two panels, h) Statistics calculated by two-way ANOVA (a, b, e) with Sidak’s multiple comparisons test or unpaired, two-tailed t -test (Mann–Whitney U -test) (c, d, g).

tracking of priming and expansion. At day 13 after immunization, MHCII^{ILC3} mice exhibited comparable priming of endogenous and myelin-specific T cells in the peripheral lymph nodes to littermate controls, and as quantified by parameters of activation, proliferation and polarization (Extended Data Fig. 8a–d). By contrast, MHCII^{ILC3} mice exhibited significantly reduced frequencies and numbers of myelin-specific T cells in the CNS, and reduced counts of IFN γ , IL-17A and TNF-producing myelin-specific T cells in the CNS relative to littermate controls (Fig. 3c, d, Extended Data Fig. 8d). Notably, MHCII^{ILC3} mice showed substantially reduced levels of immune cell infiltration in the spinal cord (Fig. 3e), and did not develop demyelinating disease in two active models of EAE (Fig. 3f) relative to littermate controls. Comparable results were also obtained when MHCII^{ILC3} mice were subjected to passive EAE (Fig. 3c, d, f, Extended Data Fig. 8e, f). These results were selective to ILC3s, as mice with a T-cell-specific deletion of *H2-Ab1* (MHCII) or a ROR γ t-specific deletion of *Aire* exhibited comparable EAE relative to littermate controls (Extended Data Fig. 8g, h). Intestinal inflammation or altered composition of the microbiota that arises in MHCII^{ILC3} mice²⁸ did not affect this protection, as EAE was comparable in wild-type mice that had intestinal inflammation induced through two different models relative to mock controls (Extended Data Fig. 8i). Moreover, MHCII^{ILC3} mice that were treated with vancomycin before and throughout EAE effectively normalized the gut microbiota, colon length, spleen weight, levels of neutrophils and CD4 T cells within the colon or mesenteric lymph nodes, yet continued to exhibit protection from EAE relative to vancomycin-treated littermate controls (Extended

Data Fig. 9a–d). There was no evidence of expansion or trapping of myelin-specific T cells in the intestine (Extended Data Fig. 9c). Therefore, antigen-presenting ILC3s are essential to promote pathological CD4 T cell responses in the CNS during neuroinflammation.

Tissue-resident ILC3s promote tolerance

Our data also indicate that antigen-presenting and tissue-resident ILC3s in the periphery retain tolerogenic potential during EAE owing to their lack of co-stimulatory molecules, and do not appear to affect the priming or expansion of autoreactive T cells (Extended Data Fig. 8a–c). Consistent with this, sort-purified ILC3s from the mesenteric lymph nodes of EAE mice did not induce the production of cytokines in myelin-specific T cells during co-culture, and this result could be reversed by cross-linking CD28 (Fig. 4a, Extended Data Fig. 6c). To test the possibility that peripheral tissue-resident ILC3s could be used to tolerize against myelin-specific T cell responses in vivo, we used a gain-of-function approach to induce myelin antigen peptide presentation in a cell-specific manner (STOP^{MOG} mice)⁴². These mice were crossed with Rorc^{cre} mice to selectively target MHCII⁺ ILC3s (ILC3^{MOG} mice). Sort purification of cDCs or B cells from STOP^{MOG} or ILC3^{MOG} mice, either at steady state or in the context of immunization, did not induce proliferation in naive myelin-specific T cells unless exogenous antigen was provided (Extended Data Fig. 9e, f). We next pre-transferred naive myelin-specific T cells into either STOP^{MOG} or ILC3^{MOG} mice and induced active EAE. At one-week after immunization, we detected

significantly increased staining of the pro-apoptotic molecule BIM in myelin-specific T cells and an overall increase in the frequency of FOXP3⁺ myelin-specific T cells within multiple peripheral lymph nodes of ILC3^{MOG} mice (Fig. 4b). To determine the physiological outcome of this tolerogenic reprogramming *in vivo*, we performed passive EAE in ILC3^{MOG} mice and observed a marked reduction in the frequency of circulating myelin-specific T cells relative to littermate controls (Fig. 4c). A similar significant reduction in the frequency and number of myelin-specific CD4 T cells was observed in the cervical lymph nodes relative to littermate controls (Fig. 4d). In the CNS of ILC3^{MOG} mice, myelin-specific CD4 T cells were significantly reduced in number and frequency, in addition to significantly reduced counts of IFN γ -, IL-17A- and TNF-producing myelin-specific T cells, relative to littermate controls (Fig. 4d, e). Consistent with this, ILC3^{MOG} mice exhibited reduced immune cell infiltrates into the spinal cord white matter (Fig. 4f) and significantly reduced levels of demyelinating disease in both the active and passive EAE models (Fig. 4g). These results were recapitulated by crossing STOP^{MOG} mice with IL-17A^{cre}, IL-17F^{cre} or IL-22^{cre} mice, mouse strains which are known to target ILC3s, and these mice showed similar protection from EAE induction (Extended Data Fig. 9g). To circumvent the potential for altered thymic selection, we used a novel tamoxifen-inducible Rorc^{creERT2} mouse crossed with STOP^{MOG} mice to generate ILC3^{IND-MOG} mice. We administered tamoxifen to adult mice one month before induction and observed that only ILC3^{IND-MOG} mice were protected from EAE (Fig. 4h). These data show the potency of peripheral and tissue-resident ILC3s in eliminating autoimmune T cells, inducing tolerance and protecting from neuroinflammation if experimentally targeted to present myelin antigen.

Our data collectively define a subset of ILC3s that infiltrate the CNS from the circulation during neuroinflammation. Given the similarities of this subset to those previously described to populate the intestine during colitis⁴³—as well as inflammatory group 2 ILCs (iILC2s) that circulate and are uniquely present during type 2 inflammation^{44,45}—we term this population inflammatory ILC3s (iILC3s) (Extended Data Fig. 10a). These findings advance our understanding of the ILC3 family, building on well-defined tissue-resident classical ILC3s that co-express T-bet and NKp46, as well as tissue-resident lymphoid tissue inducer (LTI)-like ILC3s that highly express CCR6 and CD4^{16,17} (Extended Data Fig. 10a). In the context of neuroinflammation, iILC3s are increased in the circulation, mature in the CNS, function as bona fide antigen-presenting cells and promote pro-inflammatory T cells (Extended Data Fig. 10b). Our findings are clinically relevant as we identify that iILC3s are increased in the blood and CSF of individuals with MS, although future research should clarify whether these circulating populations represent committed ILC3s or an ROR γ ⁺ progenitor^{46–48}. Our data also show that iILC3s in the CNS perform complementary but non-redundant roles with antigen-presenting cDCs that restimulate T cells after entry into the CNS^{39,49}, a process that could be regulated by the distinct localization of these cell types. Finally, our data reveal that tissue-resident LTI-like ILC3s in the periphery can be harnessed to promote T cell tolerance and prevent neuroinflammation when targeted to express cognate antigen through MHCII (Extended Data Fig. 10c). One distinguishing feature of these disparate functional properties across ILC3 subsets is IFN γ -dependent upregulation of antigen presentation and co-stimulatory pathways in the CNS-associated ILC3s. Although it is likely that these activation pathways are redundant and require further investigation, it is clear that peripheral tissue-resident ILC3s express MHCII in an IFN γ -independent manner²⁹ and that the engagement of CD28 is sufficient to block their tolerogenic functions. Our expanded model on the function of ILC3 subsets in the context of autoimmune neuroinflammation provides both a greater understanding of, and potential therapeutic opportunities for, MS and other demyelinating or neurodegenerative diseases in which self-specific T cell responses contribute to disease pathogenesis.

Online content

Any methods, additional references, Nature Research reporting summaries, source data, extended data, supplementary information, acknowledgements, peer review information; details of author contributions and competing interests; and statements of data and code availability are available at <https://doi.org/10.1038/s41586-021-04136-4>.

- Ota, K. et al. T-cell recognition of an immunodominant myelin basic protein epitope in multiple sclerosis. *Nature* **346**, 183–187 (1990).
- Dendrou, C. A., Fugger, L. & Friese, M. A. Immunopathology of multiple sclerosis. *Nat. Rev. Immunol.* **15**, 545–558 (2015).
- Togo, T. et al. Occurrence of T cells in the brain of Alzheimer's disease and other neurological diseases. *J. Neuroimmunol.* **124**, 83–92 (2002).
- Monsonego, A. et al. Increased T cell reactivity to amyloid β protein in older humans and patients with Alzheimer disease. *J. Clin. Invest.* **112**, 415–422 (2003).
- Sulzer, D. et al. T cells from patients with Parkinson's disease recognize α -synuclein peptides. *Nature* **546**, 656–661 (2017).
- Lindestam Arlehamn, C. S. et al. α -Synuclein-specific T cell reactivity is associated with preclinical and early Parkinson's disease. *Nat. Commun.* **11**, 1875 (2020).
- Lincoln, M. R. et al. A predominant role for the HLA class II region in the association of the MHC region with multiple sclerosis. *Nat. Genet.* **37**, 1108–1112 (2005).
- Hamza, T. H. et al. Common genetic variation in the HLA region is associated with late-onset sporadic Parkinson's disease. *Nat. Genet.* **42**, 781–785 (2010).
- Jansen, I. E. et al. Genome-wide meta-analysis identifies new loci and functional pathways influencing Alzheimer's disease risk. *Nat. Genet.* **51**, 404–413 (2019).
- Nalls, M. A. et al. Large-scale meta-analysis of genome-wide association data identifies six new risk loci for Parkinson's disease. *Nat. Genet.* **46**, 989–993 (2014).
- Fallis, R. J., Raine, C. S. & McFarlin, D. E. Chronic relapsing experimental allergic encephalomyelitis in SJL mice following the adoptive transfer of an epitope-specific T cell line. *J. Neuroimmunol.* **22**, 93–105 (1989).
- Brochard, V. et al. Infiltration of CD4⁺ lymphocytes into the brain contributes to neurodegeneration in a mouse model of Parkinson disease. *J. Clin. Invest.* **119**, 182–192 (2009).
- Browne, T. C. et al. IFN- γ production by amyloid β -specific Th1 cells promotes microglial activation and increases plaque burden in a mouse model of Alzheimer's disease. *J. Immunol.* **190**, 2241–2251 (2013).
- Lodygin, D. et al. β -Synuclein-reactive T cells induce autoimmune CNS grey matter degeneration. *Nature* **566**, 503–508 (2019).
- Dulken, B. W. et al. Single-cell analysis reveals T cell infiltration in old neurogenic niches. *Nature* **571**, 205–210 (2019).
- Vivier, E. et al. Innate lymphoid cells: 10 years on. *Cell* **174**, 1054–1066 (2018).
- Sonnenberg, G. F. & Hepworth, M. R. Functional interactions between innate lymphoid cells and adaptive immunity. *Nat. Rev. Immunol.* **19**, 599–613 (2019).
- Mair, F. & Becher, B. Th1⁺ Sca1⁺ innate lymphoid cells infiltrate the CNS during autoimmune inflammation, but do not contribute to disease development. *Eur. J. Immunol.* **44**, 37–45 (2014).
- Hatfield, J. K. & Brown, M. A. Group 3 innate lymphoid cells accumulate and exhibit disease-induced activation in the meninges in EAE. *Cell. Immunol.* **297**, 69–79 (2015).
- Kwong, B. et al. T-bet-dependent NKp46⁺ innate lymphoid cells regulate the onset of T_H17-induced neuroinflammation. *Nat. Immunol.* **18**, 1117–1127 (2017).
- Yamano, T. et al. Aire-expressing ILC3-like cells in the lymph node display potent APC features. *J. Exp. Med.* **216**, 1027–1037 (2019).
- Gasteiger, G., Fan, X., Dikiy, S., Lee, S. Y. & Rudensky, A. Y. Tissue residency of innate lymphoid cells in lymphoid and nonlymphoid organs. *Science* **350**, 981–985 (2015).
- Takeshita, Y. & Ransohoff, R. M. Inflammatory cell trafficking across the blood–brain barrier: chemokine regulation and *in vitro* models. *Immunol. Rev.* **248**, 228–239 (2012).
- Perry, J. S. et al. Inhibition of LTI cell development by CD25 blockade is associated with decreased intrathecal inflammation in multiple sclerosis. *Sci. Transl. Med.* **4**, 145ra106 (2012).
- Lin, Y. C. et al. Daclizumab reverses intrathecal immune cell abnormalities in multiple sclerosis. *Ann. Clin. Transl. Neurol.* **2**, 445–455 (2015).
- Degn, M. et al. Increased prevalence of lymphoid tissue inducer cells in the cerebrospinal fluid of patients with early multiple sclerosis. *Mult. Scler.* **22**, 1013–1020 (2016).
- Serafini, B. et al. ROR γ t expression and lymphoid neogenesis in the brain of patients with secondary progressive multiple sclerosis. *J. Neuropathol. Exp. Neurol.* **75**, 877–888 (2016).
- Hepworth, M. R. et al. Innate lymphoid cells regulate CD4⁺ T-cell responses to intestinal commensal bacteria. *Nature* **498**, 113–117 (2013).
- Hepworth, M. R. et al. Immune tolerance. Group 3 innate lymphoid cells mediate intestinal selection of commensal bacteria-specific CD4⁺ T cells. *Science* **348**, 1031–1035 (2015).
- von Burg, N. et al. Activated group 3 innate lymphoid cells promote T-cell-mediated immune responses. *Proc. Natl Acad. Sci. USA* **111**, 12835–12840 (2014).
- Ting, J. P. & Trowsdale, J. Genetic control of MHC class II expression. *Cell* **109**, S21–S33, (2002).
- Schroder, K., Hertzog, P. J., Ravasi, T. & Hume, D. A. Interferon- γ : an overview of signals, mechanisms and functions. *J. Leukoc. Biol.* **75**, 163–189 (2004).
- Bryant, P. W., Lennon-Dumenil, A. M., Fiebiger, E., Lagaudriere-Gesbert, C. & Ploegh, H. L. Proteolysis and antigen presentation by MHC class II molecules. *Adv. Immunol.* **80**, 71–114 (2002).
- Zhang, Q. & Vignali, D. A. Co-stimulatory and co-inhibitory pathways in autoimmunity. *Immunity* **44**, 1034–1051 (2016).

35. Lee, J. Y. et al. Serum amyloid A proteins induce pathogenic Th17 cells and promote inflammatory disease. *Cell* **180**, 79–91 (2020).
36. Koda, T. et al. Sema4A is implicated in the acceleration of Th17 cell-mediated neuroinflammation in the effector phase. *J. Neuroinflammation* **17**, 82 (2020).
37. Hur, E. M. et al. Osteopontin-induced relapse and progression of autoimmune brain disease through enhanced survival of activated T cells. *Nat. Immunol.* **8**, 74–83 (2007).
38. Giles, D. A., Duncker, P. C., Wilkinson, N. M., Washnock-Schmid, J. M. & Segal, B. M. CNS-resident classical DCs play a critical role in CNS autoimmune disease. *J. Clin. Invest.* **128**, 5322–5334 (2018).
39. Mundt, S. et al. Conventional DCs sample and present myelin antigens in the healthy CNS and allow parenchymal T cell entry to initiate neuroinflammation. *Sci. Immunol.* **4**, eaau8380 (2019).
40. Korn, T. & Kallies, A. T cell responses in the central nervous system. *Nat. Rev. Immunol.* **17**, 179–194 (2017).
41. Waisman, A. & Johann, L. Antigen-presenting cell diversity for T cell reactivation in central nervous system autoimmunity. *J. Mol. Med.* **96**, 1279–1292 (2018).
42. Frommer, F. et al. Tolerance without clonal expansion: self-antigen-expressing B cells program self-reactive T cells for future deletion. *J. Immunol.* **181**, 5748–5759 (2008).
43. Buonocore, S. et al. Innate lymphoid cells drive interleukin-23-dependent innate intestinal pathology. *Nature* **464**, 1371–1375 (2010).
44. Huang, Y. et al. IL-25-responsive, lineage-negative KLRG1^{hi} cells are multipotential ‘inflammatory’ type 2 innate lymphoid cells. *Nat. Immunol.* **16**, 161–169 (2015).
45. Huang, Y. et al. S1P-dependent interorgan trafficking of group 2 innate lymphoid cells supports host defense. *Science* **359**, 114–119 (2018).
46. Montaldo, E. et al. Human RORγt⁺CD34⁺ cells are lineage-specified progenitors of group 3 RORγt⁺ innate lymphoid cells. *Immunity* **41**, 988–1000 (2014).
47. Lim, A. I. et al. Systemic human ILC precursors provide a substrate for tissue ILC differentiation. *Cell* **168**, 1086–1100 (2017).
48. Scoville, S. D. et al. A progenitor cell expressing transcription factor RORγt generates all human innate lymphoid cell subsets. *Immunity* **44**, 1140–1150 (2016).
49. Jordao, M. J. C. et al. Single-cell profiling identifies myeloid cell subsets with distinct fates during neuroinflammation. *Science* **363**, eaat7554 (2019).

Publisher's note Springer Nature remains neutral with regard to jurisdictional claims in published maps and institutional affiliations.

© The Author(s), under exclusive licence to Springer Nature Limited 2021

Methods

Data reporting

Animal sample size estimates were determined using power analysis (power = 90% and $\alpha = 0.05$) based on the mean and standard deviation from our previous studies and/or pilot studies using at least three animals per group. The animal experiments were not randomized because littermate group allocation was performed by animal genotype; because of this, the investigators were not blinded to allocation during experiments and clinical assessment. All attempts at replication of experiments were successful and were performed at least two to three times unless otherwise noted.

Mice

Wild-type (CD45.2⁺), CD45.1⁺ (stock: 3574), H2-Ab1^{f/f} (stock: 013181)⁵⁰, 2D2 TCR^{MOG} transgenic (stock: 006912)⁵¹, Rosa-26-*loxP*-flanked STOP yellow fluorescent protein gene (eYFP) mice (stock: 006148)⁵², CD4-cre (stock: 022071)⁵³, Aire^{fl/fl} (stock: 031409)⁵⁴, *Il17a*^{Cre} (stock: 016879)⁵⁵ and *Il22*^{Cre} (stock: 027524) mice⁵⁶ on a C57BL/6J background were purchased from The Jackson Laboratory. *Rorc*^{Cre} mice and *Rorc*-eGFP⁵⁷ mice on the C57BL/6 background were provided by G.E. liMOG (STOP^{MOG})⁴² and *Il17*^{Cre} mice⁵⁸ were provided by A.W. *Rorc*-CreERT2 mice were generated by A.D. and K.G. by inserting a codon-adapted CreERT2 cassette with a Red/ET insertion kit (GeneBridges) into the transcriptional start site in exon 1 of the *Rorc* gene of RP24-14IH23 BAC (<https://bacpacresources.org>). The vector was highly purified and injected into FVB × C57BL/6NFI fertilized oocytes. Mice were crossed back onto C57BL/6N for more than 10 generations. For experiments with *Rorc*-CreERT2 mice, a 20 mg ml⁻¹ solution of tamoxifen (Sigma-Aldrich) was prepared by suspension in olive oil (Sigma-Aldrich) at 37 °C for 2 h on a shaker. liMOG × RORC^{ERT2} mice were injected intraperitoneally with 2 mg tamoxifen, 2 days apart at day -28 and -30. All mice were bred and maintained in specific-pathogen-free facilities at Weill Cornell Medicine or University Mainz and littermates were used as controls in all experiments. Sex- and age-matched mice between 8 and 12 weeks of age were used for all experiments unless otherwise indicated. No mice were excluded from the analysis unless clearly indicated. All mouse experiments were approved by, and performed in accordance with, the Institutional Animal Care and Use Committee guidelines at Weill Cornell Medicine or in accordance with the guidelines of the Central Animal Facility Institution of Mainz and in accordance with relevant laws and guidelines with permission by the state Rhineland-Palatinate (animal experimentation applications (TVA) numbers G13-1-099 and G12-1-057).

Patient consent

All participants in the RRMS study were recruited according to Weill Cornell Medicine Institutional Review Board-approved protocol no. 1003010940. Inclusion into the MS arm required a diagnosis of confirmed MS on the basis of the 2010 revised McDonald criteria⁵⁹. Individuals who had a first- or second-degree relative with a diagnosis of MS or a clinically isolated syndrome were excluded from the healthy control (HC) arm.

Inclusion criteria: (1) Individuals with clinically definite MS—male and female patients of 18 years of age or older (Supplementary Tables 1, 2) who met 2010 revised McDonald criteria. Individuals were required to have the ability to provide informed consent and be willing to participate in the study. (2) Healthy control individuals were enrolled for comparison. (3). Both patients with MS and control individuals were excluded from the study if they did not have the ability to give consent or if they had dementia. No self-selection bias or other biases were present that could affect the results.

Exclusion criteria. any individual who met the criteria below was excluded from participating in this study: (1) As part of the standard of care, individuals taking warfarin and other anticoagulants. (2) Pregnancy. (3) Body mass index greater than or equal to 35 or less than or equal to 18. (4) Use of the following medications within the last six months: systemic

antibiotics (intravenous, intramuscular or oral) for greater than three days. (5) Chronic, clinically significant (unresolved, requiring on-going medical management or medication) pulmonary, cardiovascular, gastrointestinal, hepatic or renal functional abnormality, self-reported. (6) Recent history of chronic alcohol consumption defined as more than 5 oz (or 5 drinks) of ethanol per day. (7) Any suspected state of immunosuppression or immunodeficiency including HIV. (8). History of active uncontrolled gastrointestinal disorders or diseases including (a) inflammatory bowel disease; (b) ulcerative colitis (mild–moderate–severe); (c) Crohn's disease (mild–moderate–severe); (d) indeterminate colitis; (e) irritable bowel syndrome (moderate–severe); (f) persistent, infectious gastroenteritis, colitis or gastritis; (g) *Clostridium difficile* infection (recurrent). (9) Any chronic infectious disease. (10) Haemoglobin values less than 7 or evidence of blood dyscrasia.

Individuals provided informed written consent at the Weill Cornell Medicine Multiple Sclerosis Center before sample inclusion. Healthy control samples (age- and sex-matched) (Supplementary Table 1) were obtained from healthy donors (without RRMS) at the Jill Roberts Institute for Research at Weill Cornell Medicine.

Active and passive EAE induction

We induced active EAE using a standard protocol⁶⁰. In brief, we immunized mice with 200 μ l of an emulsion containing 200 μ g myelin oligodendrocyte glycoprotein peptide (MOG_{35–55}, MEVGWYRSPF-SRVVHLYRNGK, GenScript) or recombinant MOG_{1–125} (Anaspec, AS-55150-1000) in complete Freund's adjuvant (Sigma) with 1.1 mg mycobacterium tuberculosis H37 Ra (Difco). At day 0 and day 2 after immunization, we injected 400 ng of pertussis toxin (List Biologicals) intraperitoneally. Where specified, to track MOGp-specific T cell responses in active EAE, we pre-transferred 1×10^6 naive 2D2 T cells (isolated using a MACS kit, Miltenyi Biotec) in 200 μ l retro-orbitally per mouse 24 h before induction of active EAE.

We induced passive EAE using a modified standard protocol⁶¹. In brief, we cultured bulk lymphocytes and RBC-lysis-buffer-treated splenocytes (2×10^6 cells per ml in a 24-well plate) from naive 2D2 TCR transgenic mice in complete Iscove's modified Dulbecco's medium (Thermo Fisher Scientific) containing 10% HI-FBS, penicillin–streptomycin, L-glutamine, HEPES and β -mercaptoethanol, with MOGp (25 μ g ml⁻¹), cytokines (mIL-1 β , mIL-6, mIL-23, all 10 ng ml⁻¹, Thermo Fisher Scientific) and neutralizing antibodies anti-IFN γ (XMG1.2) and anti-IL-4 (11B11) both at 5 μ g ml⁻¹. After 72 h, bulk cultures were washed once, resuspended to 2×10^6 cells per ml in complete medium with anti-CD28 (1 μ g ml⁻¹) (37.51) and mIL-23 (10 ng ml⁻¹) and transferred onto 24-well tissue culture plates pre-coated with anti-CD3 (5 μ g ml⁻¹). After 48 h, live cells were purified via Ficol and total CD4 T cells were enriched using MACS (Miltenyi Biotec). A total of 5×10^6 – 8×10^6 2D2 T cells were resuspended in 200 μ l PBS and transferred into recipient mice by retro-orbital injection. For both active and passive EAE, we weighed mice daily and scored their neurological deficits according to a standard EAE scoring scale: 0, no detectable clinical signs; 0.5, partial tail weakness; 1, tail paralysis; gait instability or impaired righting ability; 2, hind limb paresis or partial paralysis 3, full hind limb paralysis with partial fore limb paresis or paralysis; 4, hind limb and fore limb paralysis; 5, moribund.

Parabiosis surgery and EAE induction

Eight-week-old, weight-matched (± 0.5 g) female CD45.1⁺ and CD45.2⁺ mice pairs were co-housed for one week before being prepared for surgery. The parabiotic surgery was performed as previously described⁶². In brief, under continuous isoflurane, a matching incision was made from the elbow joint of the forelimb to the knee joint of the hindlimb of each mouse and bupivacaine was applied locally along incisions. Each pair was sutured with elbow and knee ligaments using non-absorbable 4–0 ethilon suture (699G) and skin was ligated using a combination of absorbable 5–0 vicryl (J463G) and removable staples between partners.

Article

Mice were given meloxicam and buprenorphine immediately before surgery and for up to 72 h after surgery. Mice were provided with Sulfratrim (antibiotic) diet for two weeks after surgery, then were placed onto a normal mouse diet. External staples and sutures were removed after healing was observed, 7–14 days after surgery. Mice-pairs were allowed to acclimate in individual cages for 6–8 weeks after surgery. Blood chimerism was confirmed through flow cytometry on PBMCs and active EAE was induced in both mice of each pair. Mice were euthanized immediately at the onset of clinical symptoms (clinical score 0.5, day 10–12 after immunization) and host- versus partner-derived immune cells were quantified by comparison of CD45.1⁺ and CD45.2⁺ staining through flow cytometry.

Isolation of cells from the blood, lymph nodes, dura meninges, CNS and intestinal lamina propria of mice

Mice were euthanized by CO₂ asphyxiation, and where indicated, blood was collected from the vena cava and transferred to 4% sodium citrate on ice. Mice were then perfused through the left ventricle of the heart with cold PBS. The intestine, lymph nodes (cervical or inguinal), dura meninges, brain and/or spinal cord (CNS indicates both tissues) were collected by dissection and held on ice-cold PBS (intestines) or complete RPMI medium containing 10% HI-FBS, penicillin–streptomycin, L-glutamine and β -mercaptoethanol unless otherwise noted. Lymph nodes were gently dissociated using a 5-ml syringe plunger through a cell strainer (70 μ m) and washed once with complete medium. Blood was washed once with complete RPMI and treated with ACK lysis buffer (A1049201), and PBMCs were then isolated by Ficoll gradient centrifugation. The CNS was minced with a sharp razor blade and digested for 20 min at 37 °C on a shaker with collagenase D (2 mg ml⁻¹; Roche Diagnostics) and DNase I (0.1 mg ml⁻¹; Sigma) in HBSS (Sigma-Aldrich). Mononuclear cells were isolated by passage through a cell strainer (70 μ m) and enriched by 30/70% Percoll gradient centrifugation (GE Healthcare). For the intestinal lamina propria, intestines were cleaned of fat tissue and washed in ice-cold PBS. Peyer's patches on the small intestine were removed and intestines were opened longitudinally and washed in PBS. Mucus was gently removed by forceps and intestines were cut into approximately 0.5-cm sections. Epithelial cells were dissociated by incubation on a shaker in HBSS containing 5 mM EDTA (Thermo Fisher Scientific), 1 mM DTT (Sigma-Aldrich) and 2% FBS twice for 20 min at 37 °C. After each step, samples were vortexed and the epithelial fraction was discarded. Afterwards, samples were washed with PBS and enzymatic digestion was performed in RPMI containing 10% FBS and 0.4 U ml⁻¹ dispase (Thermo Fisher Scientific), 1 mg ml⁻¹ collagenase III (Worthington) and 20 μ g ml⁻¹ DNase I (Sigma-Aldrich) on a shaker for 45 min at 37 °C. Leukocytes were further enriched by 40/80% Percoll gradient centrifugation.

Isolation, storage and preparation of human PBMCs and tonsils

PBMCs were isolated through density-gradient Ficoll centrifugation of blood samples. Ficoll-spun buffy coats were collected within hours of peripheral blood draws and cryopreserved in FBS containing 10% dimethyl sulfoxide (DMSO). On the day of the flow cytometry experiment, samples were rapidly thawed and washed once with RPMI containing 20% FBS immediately before staining for flow cytometry. Human tonsil samples were provided by the Cooperative Human Tissue Network (CHTN), which is funded by the National Cancer Institute. Other investigators may have received specimens from the same individuals. Single-cell suspensions were isolated from the tonsil by dissociating samples through a 70- μ m cell strainer. Cells were viably cryopreserved at -150 °C in 90% FBS and 10% DMSO for future analyses.

Flow cytometry and cell sorting

Single-cell suspensions were incubated on ice with conjugated antibodies in PBS containing 2% FBS and 1 mM EDTA. Dead cells were excluded with Fixable Aqua Dead Cell Stain (Thermo Fisher Scientific) for flow

cytometry or Sytox Blue Dead Cell Stain (1:1,000) (Thermo Fisher Scientific) for cell sorting added during surface staining. The staining antibodies for flow cytometry (all used at 1:200 unless otherwise indicated) were purchased from Thermo Fisher Scientific, Biolegend or BD Biosciences. For mouse cell-surface staining: B220 (RA3-6B2), CCR6 (29-2L17), CD3 ϵ (145-2C11), CD4 (GK1.5, RM4-5), CD5 (53-7.3), CD8 α (53-6.7), CD11b (M1/70), CD11c (N418), CD19 (eBio1D3), CD25 (PC61), CD30L (RM153), CD40 (3/23), CD44 (IM7), CD45 (30-F11), CD45.1 (A20), CD45.2 (104), CD62L (MEL-14), CD64 (X54-5/7.1), CD80 (16-10A1), CD86 (GL-1), CD90.2 (Thy1.2) (30-H12, 53-H12), CD127 (A7R34), CD172a (P84), F4/80 (BM8), KLRG1 (2F1), Ly6C (HK1.4), Ly6G (IA8), MHCII (M5/114.15.2, 2G9), NKp46 (29A1.4), NK1.1 (PK136), OX40L (RM134L), Thy1.1 (OX-7, HIS51) and XCR1 (ZET). For mouse intracellular staining: FOXP3 (FJK-16S), IL-17A (eBio 17B7), IFN γ (XMG1.2), Ki-67 (SolA15), ROR γ t (B2D), T-bet (eBio4B10), GM-CSF (MP1-22E9), BIM (C34C5) and TNF (MP6-XT22). For human surface staining: CD19 (HIB19), CD94 (DX22) (1:50), CD14 (M5E2), CD123 (6H6), FcR1a (AER-37(CRA1)), CD11c (BU15) (1:100), HLA-DR (L243), CD86 (BU63), CD80 (L307.4), cKit (104D2) (1:100), CD127 (A019D5) (1:100), CD3 (UCHT1) (1:50), CD4 (SK3) (1:100), CD45 (HI30) (1:50) and CRTH2 (BM16) (1:50). For human intracellular staining: ROR γ t (Q21-559) (1:50).

Unless otherwise noted, for intracellular transcription factor or cytokine staining, cells were stained for surface markers, followed by fixation and permeabilization according to the manufacturer's protocol (FOXP3 staining buffer set from Thermo Fisher Scientific). For intracellular transcription factor staining in cells isolated from Rorc-cre^{eYFP} mice, cells were stained for surface markers, then cells were fixed using the BD Cytofix/Cytoperm Fixation/Permeabilization Kit (554714) for one hour on ice, washed with the Thermo Fisher Scientific permeabilization buffer and stained for transcription factors overnight at room temperature before flow cytometry analysis.

For intracellular cytokine staining, cells were first incubated for 4 h in RPMI with 10% FBS, 50 ng ml⁻¹ phorbol 12-myristate 13-acetate (PMA), 750 ng ml⁻¹ ionomycin and 10 μ g ml⁻¹ brefeldin A, all obtained from Sigma-Aldrich. Fluorophore conjugates are indicated on figures. All flow cytometry experiments were performed using a LSR Fortessa flow cytometer and the FACS Diva software (BD Biosciences) and analysed with FlowJo v.10 software (Tree Star) or sort-purified using a FACS Aria II cell sorter (BD Biosciences).

RNA sequencing

ILC3s (CD45⁺CD3 ϵ ⁻CD5⁻CD8 α ⁻NK1.1⁻CD11b⁻CD11c⁻CD19⁻CD127⁺CD90.2⁺ROR γ t(GFP)⁺) (0.5–1 \times 10³ per tissue per mouse) were sort-purified from Rorc-eGFP mice at day 15 of active EAE. Sorted cells were used to prepare RNA-sequencing libraries by the Epigenomics Core at Weill Cornell Medicine, using the Clontech SMARTer UltraLow Input RNA Kit V4 (Clontech Laboratories). Sequencing was performed on an Illumina HiSeq 4000, yielding 50-bp single-end reads. Raw sequencing reads were demultiplexed with Illumina CASAVA (v.1.8.2). Adapters were trimmed from reads using FLEXBAR (v.2.4) and reads were aligned to the NCBI GRCm38/mm10 mouse genome using the STAR aligner (v.2.3.0) with default settings. Reads per gene were counted using Rsubread. Genes with at least ten counts in each sample were considered for further analysis. Differential expression was assessed using DESeq2 v.1.14.0 with default parameters and with a false discovery rate (FDR) of 0.1. Principal component analysis was performed after using DESeq2 variance stabilizing transformation. Heat maps of the normalized gene counts, represented either as log₂(1 + x) or z-score, were generated using Morpheus (<https://software.broadinstitute.org/morpheus>).

Antibiotic administration and faecal 16S rRNA sequencing

Vancomycin hydrochloride (Chem-Impex International, 00315) was dissolved (0.25 mg ml⁻¹) in autoclaved deionized water and provided in the cage drinking water before and throughout induction of EAE. Faecal pellets were collected before administration of vancomycin

and at 7 days later (one day before induction of EAE). Faecal samples and subsequent sequencing were performed by the Microbiome Core Laboratory of Weill Cornell Medicine: Faecal pellets were deposited into Qiagen PowerBead glass 0.1-mm tubes (13118-50). Using a Promega Maxwell RSC PureFood GMO and Authentication Kit (AS1600), 1 ml of CTAB buffer and 20 μ l of RNase A solution was added to the PowerBead tube containing each sample. The sample and buffer were mixed for 10 s on a Vortex Genie2 and then incubated at 95 °C for 5 min on an Eppendorf ThermoMixer F2.0, shaking at 1,500 rpm. The tube was removed and clipped to a horizontal microtube attachment on a Vortex Genie2 (SI-H524) and vortexed at high speed for 20 min. The sample was removed from the Vortex and centrifuged on an Eppendorf Centrifuge 5430R at 40 °C, 12,700 rpm for 10 min. After completion, the sample was centrifuged again for an additional 10 min to eliminate foam. The sample tube cap was removed, and the sample checked for foam and particulates. If foam or particulates were found in the sample, they were carefully removed using a P1000 pipette. The opened tube was then added to a Promega MaxPrep Liquid Handler tube rack. The Liquid Handler instrument was loaded with proteinase K tubes, lysis buffer, elution buffer, 1,000-ml tips, 50-ml tips, 96-sample deep-well plate, and Promega Maxwell RSC 48 plunger tips. The Promega MaxPrep Liquid Handler instrument was programmed to use 300 μ l of sample and transfer all sample lysate into Promega Maxwell RSC 48 extraction cartridge for DNA extraction. After completion, the extraction cartridge was loaded into the Promega Maxwell RSC 48 for DNA extraction and elution. DNA was eluted in 100 μ l and transferred to a standard 96-well plate. DNA was quantified using the Quant-iT dsDNA High Sensitivity Assay Kit using a Promega GloMax plate reader on a microplate (655087). Library generation followed the protocol from Earth Microbiome Project (<https://earthmicrobiome.org/protocols-and-standards/16s/>). Amplicon libraries were washed using Beckman Coulter AMPure XP magnetic beads. Library quality and size verification was performed using a PerkinElmer LabChip GXII instrument with the DNA IK Reagent Kit (CLS760673). Library concentrations were quantified using the Quant-iT dsDNA High Sensitivity Assay Kit using a Promega GloMax plate reader on a microplate (655087). Library molarity was calculated on the basis of library peak size and concentration. Libraries were normalized to 2 nM using the PerkinElmer Zephyr G3 NGS Workstation (133750) and pooled together using the same volume across all normalized libraries into a 1.5-ml Eppendorf DNA tube (022431021). Pooled libraries were sequenced on the Illumina MiSeq instrument at a loading concentration of 8 pM with 10% PhiX, paired-end 250 using the MiSeq Reagent Kit v2, 500-cycles (MS-102-2003). Demultiplexed raw reads were processed to generate an operational taxonomic unit (OTU) table using USEARCH v.11.0.66763. Forward and reverse reads were merged using a maximum of 5 mismatches in the overlap region, a minimum sequence identity in the overlap region of 90%, a minimum overlap length of 16 base pairs and a minimum merged sequence length of 300 base pairs. PhiX contamination was then removed, followed by quality filtering based on FASTQ quality scores, with a maximum expected error number of 1.0. OTU clustering was performed using usearch -cluster_otus with default settings. Merged (pre-filter) reads were mapped to the OTU sequences to generate the OTU table. Taxonomic classification of OTU representative sequences was performed using usearch -sintax, an implementation of the SINTAX algorithm⁶⁴, using version 16 of the Ribosomal Database Project (RDP) Training Set⁶⁵. Alpha diversity estimation and principal coordinate analysis (PCoA) were performed using the phyloseq R package⁶⁶. A phylogenetic tree was generated from the OTU representative sequences using usearch -cluster_aggd with default settings.

Myelin basic protein uptake assay

Myelin basic protein (Sigma, M1891) was conjugated to the pH-sensitive dye pHrodo Red, succinimidyl ester (Thermo Fisher Scientific, P36014), per the manufacturer's protocol, and stored at 4 °C. ILC3s were isolated

from the CNS at day 19 EAE and cultured for 2 h at 4 °C or 37 °C with pHrodo Red-labelled myelin-basic protein (50 μ g ml⁻¹ in complete medium). Cells were collected, washed, stained for viability with Aqua Dead Cell Stain and then assayed by flow cytometry. The degree of uptake was determined by pHrodo Red fluorescence in the PE channel.

Co-culture of myelin-specific T cells with antigen-presenting cells

A total of 1×10^6 naive 2D2 T cells per mouse were pre-transferred into Rorc-eGFP mice followed by induction of active EAE. On day 19 after immunization, 2D2s (CD45⁺CD90.1⁺CD4⁺), ILC3s (CD45⁺CD3 ϵ ⁺CD4⁺CD5⁺CD8 α ⁺TCR γ δ ⁺NK1.1⁻CD11b⁻CD11c⁻F4/80⁻Ly6C⁻CD19⁻CD127⁻CD90.2⁻ROR γ t-GFP⁻) or cDCs (CD45⁺CD11c⁺CD3 ϵ ⁻CD5⁻CD8 α ⁻TCR γ δ ⁻NK1.1⁻F4/80⁻Ly6C⁻CD19⁻CD90.2⁻) were sort-purified from either the CNS or the mesenteric lymph nodes. ILC3s or cDCs (1×10^3 antigen-presenting cells (APCs) per well) were incubated for 1 h at 37 °C with MOGp₃₅₋₅₅ (10 μ g ml⁻¹) or full-length recombinant MOGp₁₋₁₂₅ (2.5 μ g ml⁻¹) \pm anti-MHCII blocking antibody (5 μ g ml⁻¹) (Thermo Fisher Scientific, 16-5321-85) or anti-CD28 antibody (1 μ g ml⁻¹) (BD Biosciences, 553294). 2D2 T cells were added to wells at a ratio of 1:2 (2×10^3 2D2 T cells per well) and were incubated at 37 °C for 72 h. Co-cultures were treated with PMA-Iono-BFA for 4 h before staining for flow cytometry and intracellular cytokines.

Dendritic cell, B cell and T cell co-culture from IiMOG mice

Splenic CD11c⁺ DCs (live, CD45⁺CD90.2⁻CD19⁻B220⁻CD11c⁺MHCII⁺) or B cells (live, CD45⁺CD19⁺B220⁺) were sort-purified from either STOP^{MOG} or ILC3^{MOG} mice (after indicated treatment) and co-cultured, at the ratio 1:10 and 1:1 respectively, with 1×10^5 2D2 T cells (CD4 MACS-purified) previously stained with CellTrace Violet (CTV) dye (Thermo Fisher Scientific) at 37 °C. After 72 h, the proliferation of 2D2 T cells was assessed by measuring the dilution of CTV dye by flow cytometry.

Histological analyses of dura, brain and spinal cord

For histological analysis, freshly isolated mouse spinal cords were carefully dissected in whole starting from the lower cervical (around C5–C6) to the upper lumbar vertebrae (around L5–L6). For H&E, whole spinal cords were fixed in 4% paraformaldehyde for at least 48 h, transferred into 70% ethanol and embedded in paraffin, and 5- μ m transverse or longitudinal sections were stained with H&E. For immunofluorescence analysis, mice were perfused with 30 ml of DBPS through the left ventricle to deplete circulating cells, and whole brains or spinal cords from Rorc-eGFP mice during EAE were isolated. Tissue samples were fixed in 4% paraformaldehyde at room temperature for 1 h, washed three times in PBS and then transferred into 30% sucrose (w/v) in PBS overnight to dehydrate. Dehydrated tissues were cryoprotected in OCT medium (Tissue-Tek) and stored at -80 °C until sectioning at a thickness of 10 μ m using a cryotome (Leica Instruments) and immobilization on Superfrost Plus slides (VWR). Immobilized tissues were then stored at -20 °C until immunostaining. Slides were allowed to come to room temperature and excess OCT medium was washed off in PBS before blocking in PBS with 5% normal goat serum, 5% normal donkey serum (both Jackson ImmunoResearch) and 0.1% Triton X-100 for 30 min. Tissue sections were then stained with the following primary antibodies diluted in blocking buffer overnight at 4 °C: anti-GFP 1:200 (Abcam 6556), anti-CD3 1:50 (Biolegend clone 17A2), anti-CD11c 1:50 (eBioscience clone N418). Sections were washed three times with PBS and then incubated with secondary antibodies (anti-rabbit IgG-A488, anti-rat IgG-A555, anti-hamster IgG-647, Invitrogen) diluted 1:500 in blocking buffer for 1 h at room temperature. Tissue sections were then washed three times in PBS, incubated with DAPI (Invitrogen) for 5 min before a final wash in PBS and mounted with Prolong Gold antifade reagent (Invitrogen). For whole-mount meninges imaging, the skull cap was isolated from Rorc-eGFP mice and fixed overnight in 2% PFA, and the whole dura meninges was isolated and stained as previously

Article

described⁶⁷, using the same antibodies and concentrations above. Stained sections and whole-mount meninges were imaged on an Olympus FV1000 laser-scanning confocal microscope.

Statistical analysis

P values of datasets were determined by unpaired, or paired (where applicable), two-tailed *t*-test with a 95% confidence interval. Variance was analysed using an *F*-test. Where appropriate, Mann–Whitney *U*-test or one or two-way ANOVA followed by Sidak post-hoc tests were performed. All statistical tests were performed with Graph Pad Prism v.8 software. *P* values of less than 0.05 were considered to be significant.

Reporting summary

Further information on research design is available in the Nature Research Reporting Summary linked to this paper.

Data availability

ILC3 RNA-sequencing data are available at the Gene Expression Omnibus under accession number GSE165580. Faecal 16S data are deposited at the NCBI Sequence Read Archive under BioProject accession number PRJNA761714. Source data are provided with this paper.

50. Hashimoto, K., Joshi, S. K. & Koni, P. A. A conditional null allele of the major histocompatibility IA-beta chain gene. *Genesis* **32**, 152–153 (2002).
51. Bettelli, E. et al. Myelin oligodendrocyte glycoprotein-specific T cell receptor transgenic mice develop spontaneous autoimmune optic neuritis. *J. Exp. Med.* **197**, 1073–1081 (2003).
52. Srinivas, S. et al. Cre reporter strains produced by targeted insertion of *EYFP* and *ECFP* into the *ROSA26* locus. *BMC Dev. Biol.* **1**, 4 (2001).
53. Lee, P. P. et al. A critical role for Dnmt1 and DNA methylation in T cell development, function, and survival. *Immunity* **15**, 763–774 (2001).
54. Dobes, J. et al. A novel conditional *Aire* allele enables cell-specific ablation of the immune tolerance regulator *Aire*. *Eur. J. Immunol.* **48**, 546–548 (2018).
55. Hirota, K. et al. Fate mapping of IL-17-producing T cells in inflammatory responses. *Nat. Immunol.* **12**, 255–263 (2011).
56. Ahlfors, H. et al. IL-22 fate reporter reveals origin and control of IL-22 production in homeostasis and infection. *J. Immunol.* **193**, 4602–4613 (2014).
57. Lochner, M. et al. In vivo equilibrium of proinflammatory IL-17⁺ and regulatory IL-10⁺ Foxp3⁺ RORγ⁺ T cells. *J. Exp. Med.* **205**, 1381–1393 (2008).
58. Croxford, A. L., Kurschus, F. C. & Waisman, A. Cutting edge: an IL-17-Cre^{EYFP} reporter mouse allows fate mapping of Th17 cells. *J. Immunol.* **182**, 1237–1241 (2009).
59. Polman, C. H. et al. Diagnostic criteria for multiple sclerosis: 2010 revisions to the McDonald criteria. *Ann. Neurol.* **69**, 292–302 (2011).
60. Miller, S. D., Karpus, W. J. & Davidson, T. S. Experimental autoimmune encephalomyelitis in the mouse. *Curr. Protoc. Immunol.* **88**, 15.1.1–15.1.20 (2010).
61. Lee, Y. et al. Induction and molecular signature of pathogenic TH17 cells. *Nat. Immunol.* **13**, 991–999 (2012).
62. Kamran, P. et al. Parabiosis in mice: a detailed protocol. *J. Vis. Exp.* **80**, e50556 (2013).
63. Edgar, R. C. Search and clustering orders of magnitude faster than BLAST. *Bioinformatics* **26**, 2460–2461 (2010).
64. Edgar, R. C. SINTAX: a simple non-Bayesian taxonomy classifier for 16S and ITS sequences. Preprint at <https://doi.org/10.1101/074161> (2016).
65. Cole, J. R. et al. Ribosomal Database Project: data and tools for high throughput rRNA analysis. *Nucleic Acids Res.* **42**, D633–D642 (2014).
66. McMurdie, P. J. & Holmes, S. phyloseq: an R package for reproducible interactive analysis and graphics of microbiome census data. *PLoS ONE* **8**, e61217 (2013).
67. Louveau, A., Filiano, A. J. & Kipnis, J. Meningeal whole mount preparation and characterization of neural cells by flow cytometry. *Curr. Protoc. Immunol.* **121**, e50 (2018).

Acknowledgements We thank members of the Sonnenberg laboratory for discussions and critical reading of the manuscript; the Microbiome Core and Epigenomics Core of Weill Cornell Medicine and G. G. Putzel for technical assistance; C. Gai of Weill Cornell's Center of Comparative Medicine and Pathology (CCMP) for performing the parabiosis surgeries; and I. Ivanov of Columbia University for sharing mouse lines. The Sonnenberg laboratory is supported by the National Institutes of Health (R01AI143842, R01AI123368, R01AI145989, R01AI162936, R21CA249284 and U01AI095608), the National Institute of Allergy and Infectious Diseases (NIAID) Mucosal Immunology Studies Team (MIST), the Crohn's and Colitis Foundation, the Searle Scholars Program, the American Asthma Foundation Scholar Award, Pilot Project Funding from the Center for Advanced Digestive Care (CADC), an Investigators in the Pathogenesis of Infectious Disease Award from the Burroughs Wellcome Fund, a Wade F.B. Thompson–Cancer Research Institute (CRI) CLIP Investigator grant, the Meyer Cancer Center Collaborative Research Initiative, the Dalton Family Foundation, L. and G. Greenberg, and the Jill Roberts Institute for Research in Inflammatory Bowel Disease. G.F.S. is a CRI Lloyd J. Old STAR. J.B.G. is supported by the NIAID of the National Institutes of Health under award number F31AI138389-01A1; A.M.J. is supported by T32DK116970; and the Waisman laboratory is supported by the Deutsche Forschungsgemeinschaft (DFG) grants AW1600/10-1, AW1600/11-1 and AW1600/14-1, as well as by the National Multiple Sclerosis Society (NMSS) grant RG 1707-28780.

Author contributions J.B.G. and G.F.S. conceived the project. J.B.G. performed most of the experiments and analysed the data. A.S., T.R., A.A. and A.M.J. also helped to process tissues, generated experimental datasets and analysed data from EAE in liMOG mice (A.S. and T.R.) or Rorc^{cre} mice (A.A. and A.M.J.). C.N.P. processed tissues and generated the immunofluorescence data. M.M. coordinated the selection and T.V. provided and supervised the selection and analysis of samples from patients with RRMS, as well as providing scientific discussion. G.E., K.G. and A.D. provided essential mouse models, scientific advice and expertise. A.W. jointly supervised the research, provided essential mouse strains and contributed to the formation of the project. J.B.G. and G.F.S. wrote the manuscript, with input from all of the authors.

Competing interests The authors declare no competing interests.

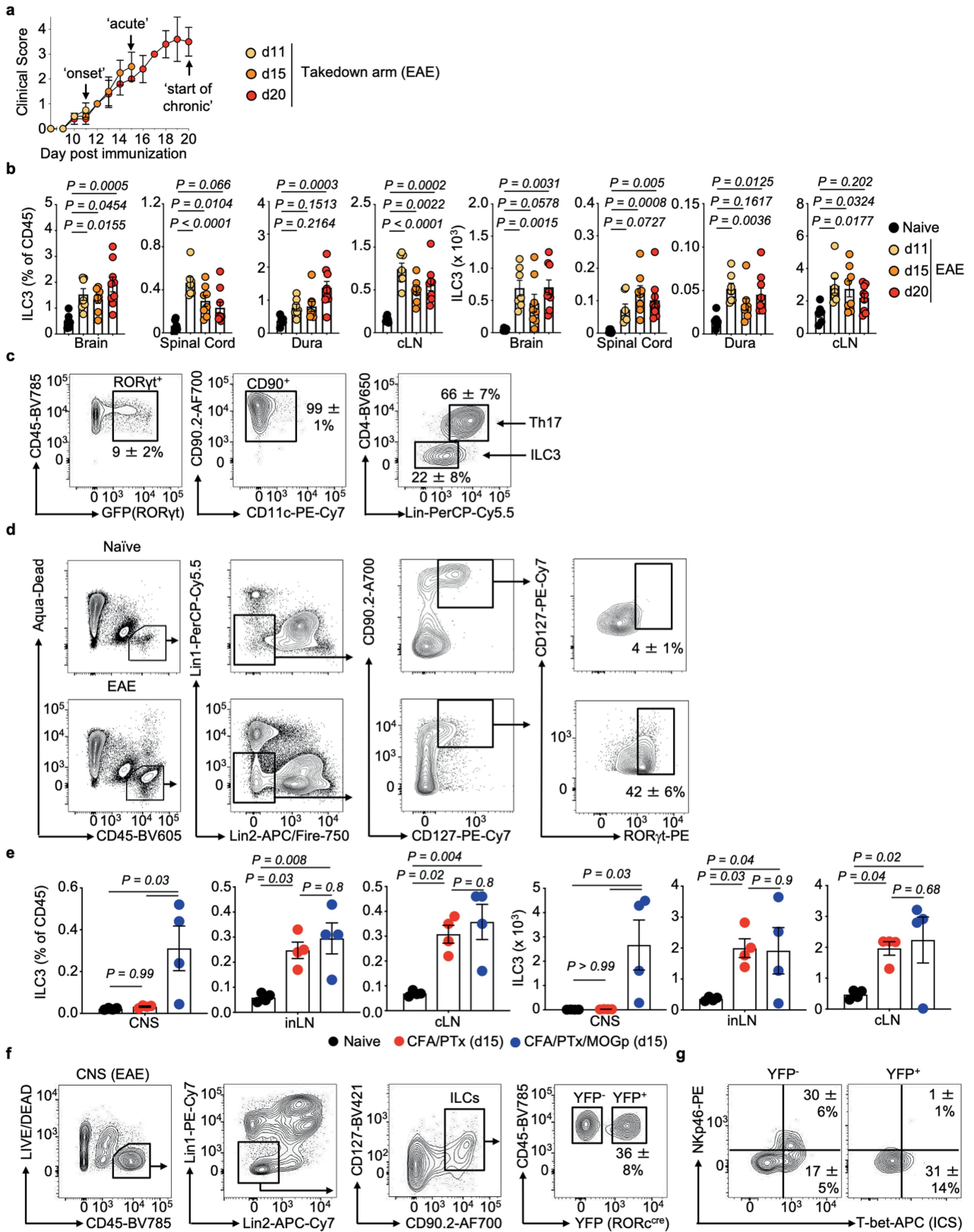
Additional information

Supplementary information The online version contains supplementary material available at <https://doi.org/10.1038/s41586-021-04136-4>.

Correspondence and requests for materials should be addressed to Gregory F. Sonnenberg.

Peer review information Nature thanks the anonymous reviewers for their contribution to the peer review of this work.

Reprints and permissions information is available at <http://www.nature.com/reprints>.

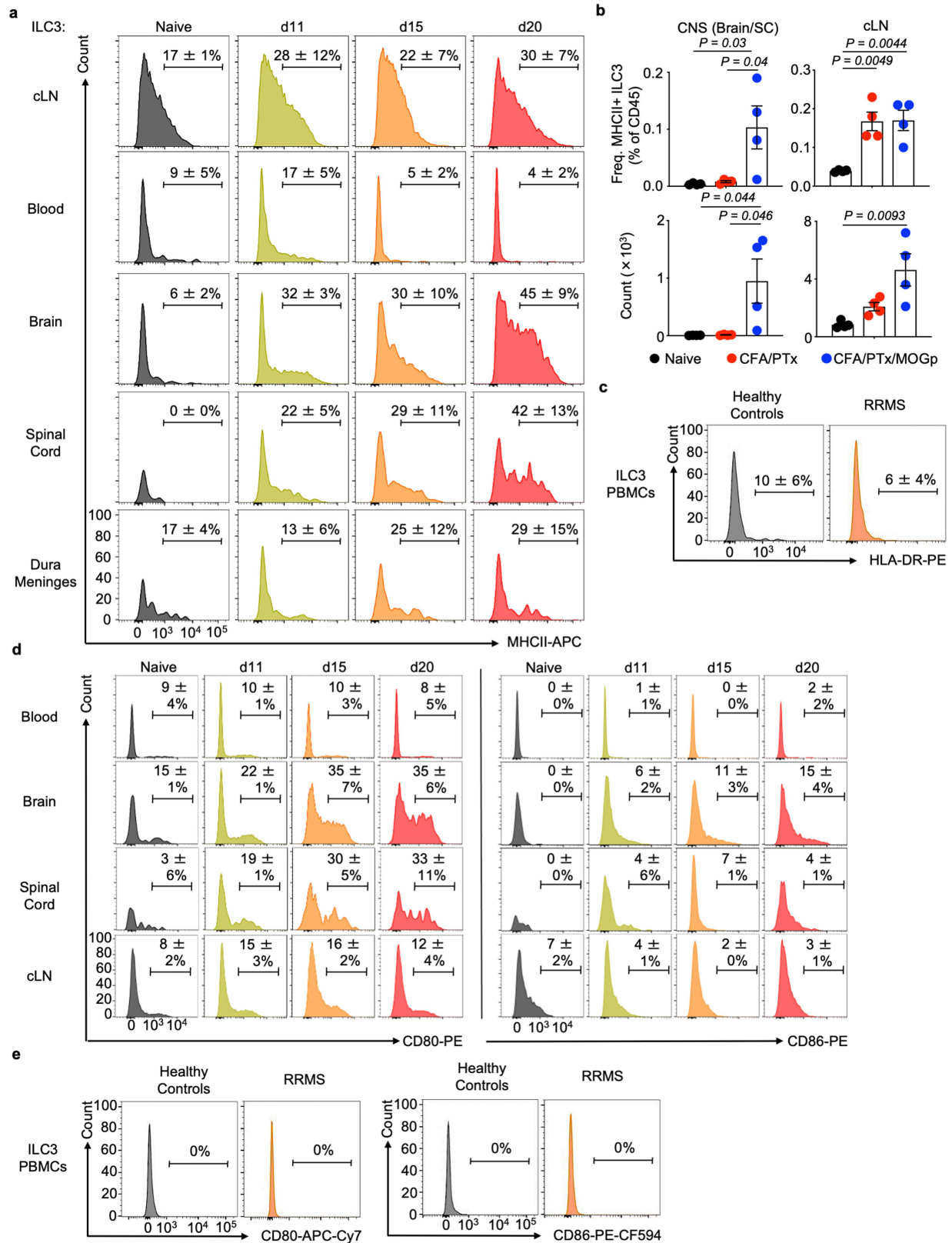


Extended Data Fig. 1 | See next page for caption.

Article

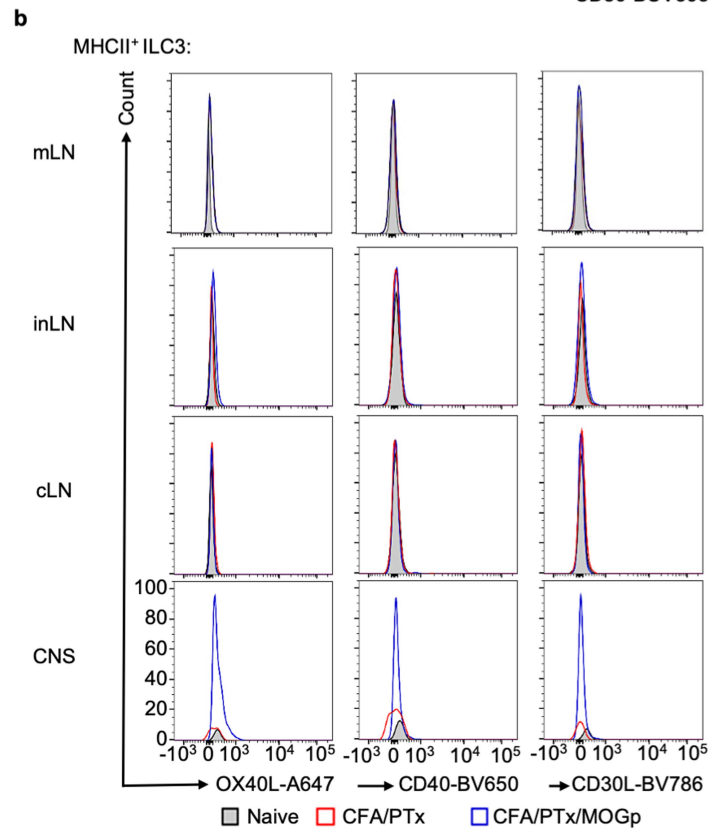
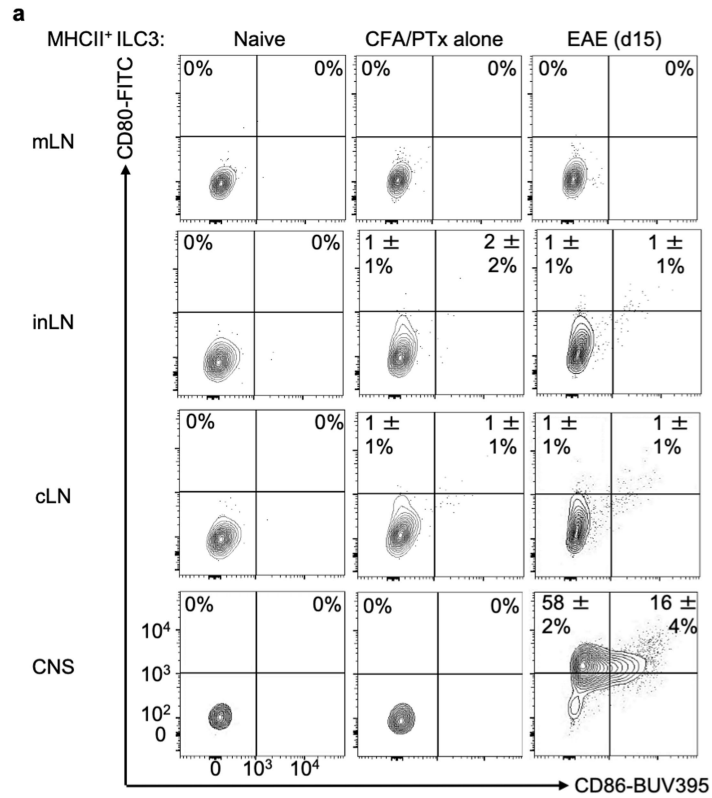
Extended Data Fig. 1 | Characterization of ILC3s in the CNS. **a**, Representative time course and clinical disease categorization of active EAE (n = 4, 5 mice/ timepoint). **b-c**, Quantification of ILC3 frequency and absolute counts within indicated tissues at steady state (Naive) (n = 6 mice) versus EAE onset (d11, n = 7), acute (d15, n = 8) or chronic (d20, n = 9) phase (**b**) and reverse flow cytometry gating strategy defining all GFP⁺ cells in the CNS (d15) (n = 4 mice/group) (**c**) during EAE in Rorc-eGFP mice. **d-e**, Naive C57BL/6 mice (n = 4 mice/group) were immunized with either PBS (Naive), CFA/PTx alone, or with CFA/PTx/MOGp. At day 15 post-immunization, ILC3s in the CNS, inLN and cLN were enumerated by flow cytometry: **d**, Representative flow cytometry gating strategy for ILC3s in

CNS (Lin1 = CD3, CD5, CD8, Lin2 = CD11b, CD11c, B220), **e**, Quantitation of frequencies and absolute counts of ILC3s. **f-g**, Representative flow cytometry on YFP⁺ ILCs (**f**) and quantification of differential expression of ILC heterogeneity in YFP⁺ ILCs (**g**) in the CNS of Rorc-cre^{eYFP} mice during active EAE (n = 6 mice/group) (Lin1 = B220, CD11b, CD11c, Lin2 = CD3e, CD5, CD8, Ly6C). Data in **a-f** are representative of two independent experiments with similar results and data in **b** are pooled from two independent experiments. Results are shown as mean ± s.d. Statistics are calculated by one-way (**b, e**) analysis of variance (ANOVA) with Sidak's multiple comparisons test.



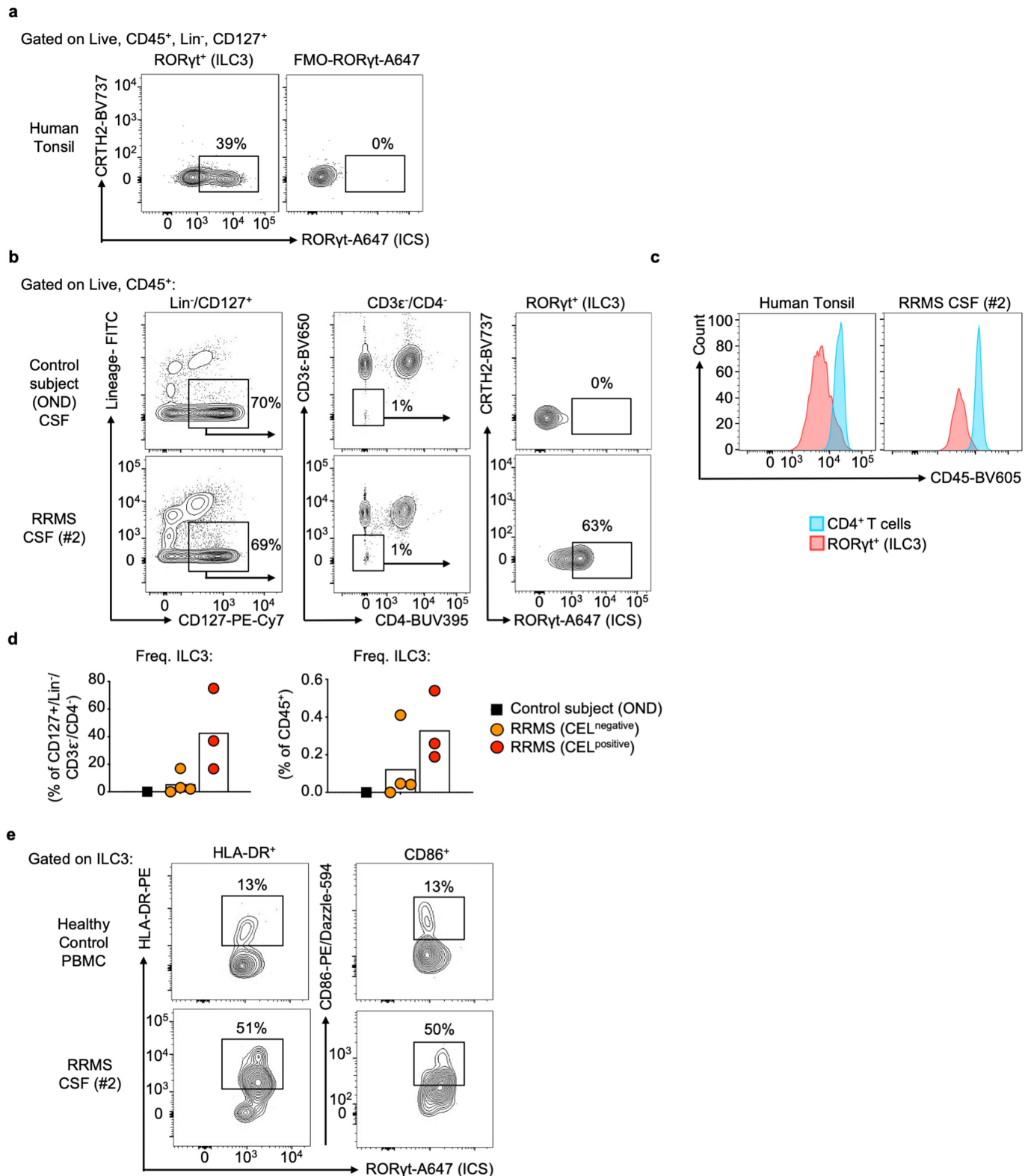
Extended Data Fig. 3 | Expression of MHCII and co-stimulatory molecules on ILC3s during neuroinflammation. a, d, Representative histograms and quantification of MHCII (a), and CD80 or CD86 (d) expression on ILC3s in indicated tissues of Rorc-eGFP mice at steady state (Naive) (n = 3 mice) versus EAE onset (d11, n = 4), acute (d15, n = 4) or chronic (d20, n = 5) phase. **b**, Naive C57BL/6 mice were immunized with either PBS (Naive), CFA/PTx or with CFA/PTx/MOGp (n = 4 mice/group). At day 15 EAE, frequency and counts of

MHCII⁺ ILC3s in the CNS and cLN were enumerated by flow cytometry. **c, e** Representative staining and quantification of HLA-DR (c) and co-stimulatory molecules (e) on human blood ILC3s (n = 18 samples/group). Data in **a, b, d** are representative of two independent experiments with similar results. Results are shown as mean ± s.d. Statistics are calculated by one-way analysis of variance (ANOVA) with Sidak's multiple comparisons test.



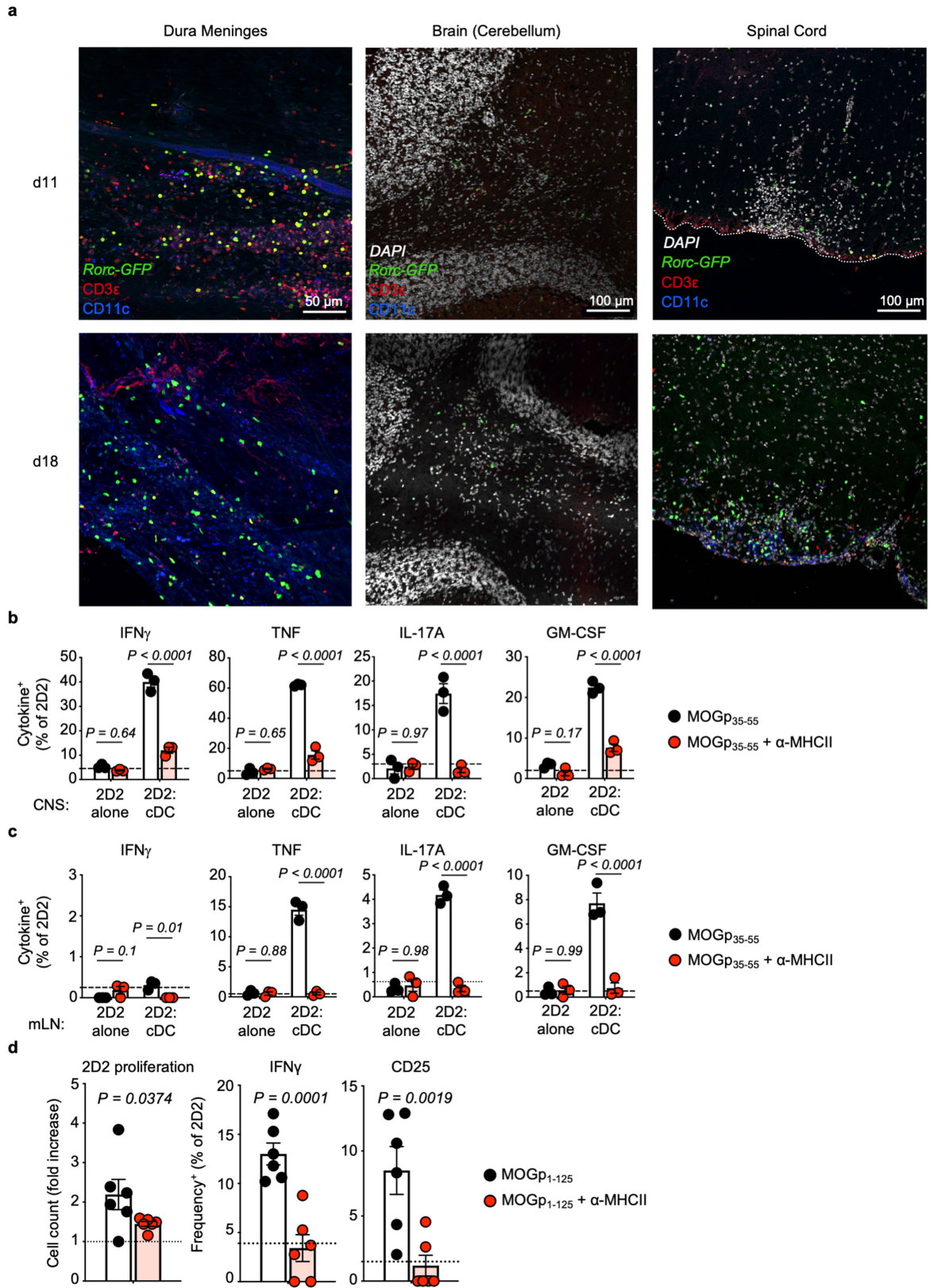
Extended Data Fig. 4 | ILC3s in the periphery do not express co-stimulatory molecules. a-b. Naive C57BL/6 mice were immunized with either PBS (Naive), CFA/PTx or with CFA/PTx/MOGp (EAE) (n = 4 mice/group). At day 15 post immunization, expression of co-stimulatory molecules CD80, CD86 (a) and

OX40L, CD40, and CD30L (b) by MHCII⁺ ILC3s in the mLN, inLN, cLN and CNS were enumerated by flow cytometry. Data are representative of three independent experiments with similar results. Results are shown as mean ± s.d.



Extended Data Fig. 5 | ILC3s are found in the cerebral spinal fluid of patients with RRMS and express HLA-DR and CD86. a, Validation of anti-RORyt antibody staining on single cell suspensions from human donor tonsils compared to FMO (Fluorescence Minus One) control indicating staining without anti-RORyt antibody. **b-e,** Cerebral spinal fluid (CSF) was obtained from 7 patients with RRMS and one control individual (other neurological disease, OND). Individuals were further stratified by the presence or absence of contrast enhancing lesions (CEL) as well as CEL number (Supplementary Table 2). CSF was processed immediately by centrifuging for 10 min at 400 x g

and staining for ILC3s as indicated (**b**) (Lineage = CD19, CD94, CD14, CD123, FcR1a, CD11c). Gated RORyt⁺ populations in the indicated tissues exhibited dim staining for CD45, which is a defining feature of ILC3s, relative to CD4 T cells (**c**). Indicated frequencies of ILC3s in the CSF were quantified (**d**). PBMCs were used as controls during each collection and used for comparison of HLA-DR or CD86 expression on ILC3s in the CSF (**e**). Results are shown as mean (**d**) and RRMS flow cytometry is representative flow cytometry from CSF of patient #2 (Supplementary Table 2). Human tonsil data is representative of 3 individual tonsil samples.

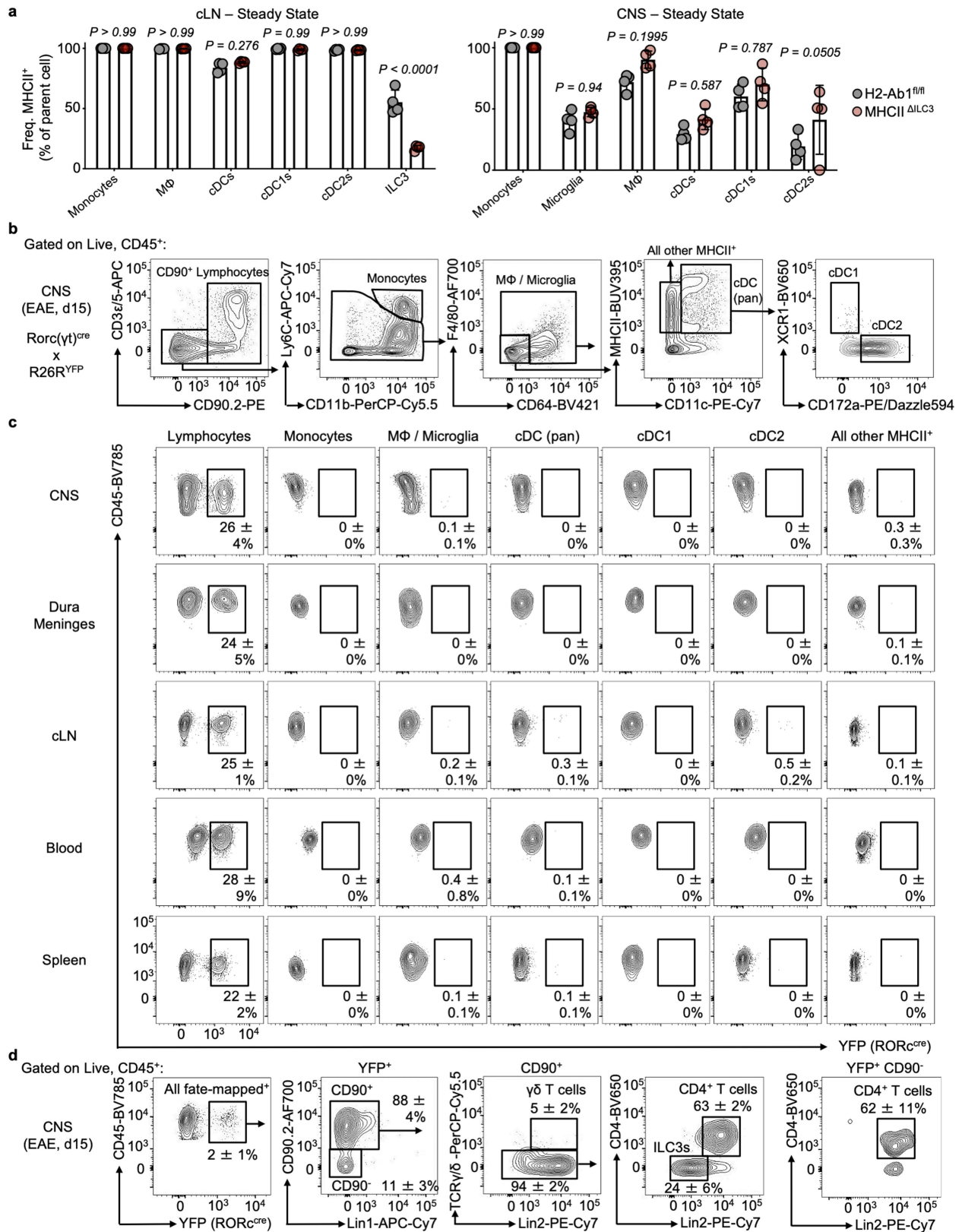


Extended Data Fig. 6 | See next page for caption.

Article

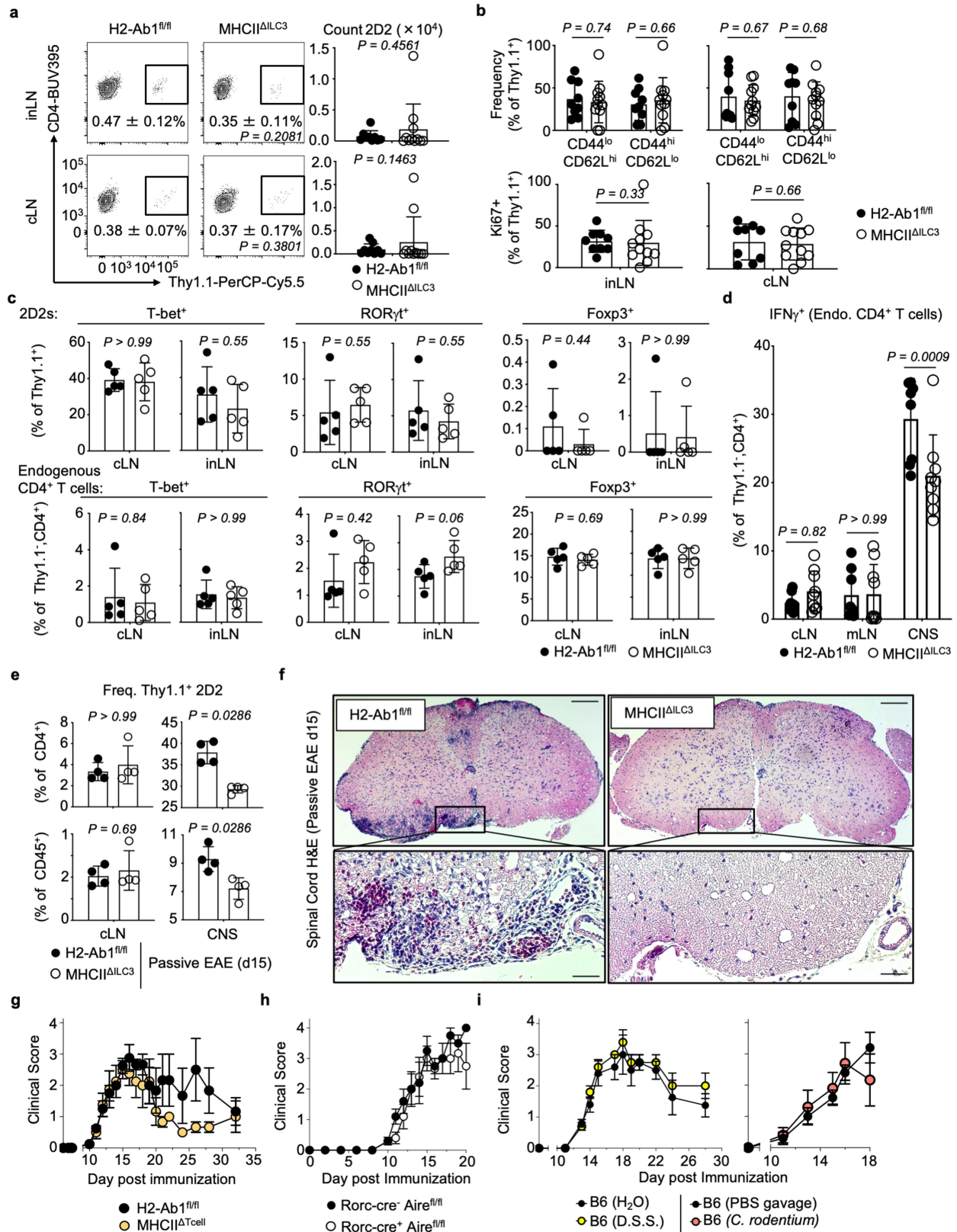
Extended Data Fig. 6 | Interrogation of ILC3 and T cell interactions in the CNS. **a**, Representative immunofluorescence staining of fixed dura meninges, brain cerebellum and spinal cord (edge denoted by dashed white line) from Rorc-eGFP mice during day 11 or day 18 of active EAE showing enrichment of GFP⁺ cells in focal lesions of the parenchyma (representative of n = 3 mice/ timepoint). **b-c**, Frequency of cytokine producing 2D2 T cells after 72 h co-culture with *ex vivo* sorted cDC or alone (2D2 T cells alone) from the CNS (**b**) or the mLN (**c**) (pooled from 5 mice, d18 EAE) in the presence of MOGp +/- α -MHCII blocking antibody. **d**, To determine the ability to process full-length antigen 2D2 T cells and ILC3s were sorted from the CNS (pooled from n = 5 mice, d19 EAE) and co-cultured as indicated for 72 h prior to determination of

cell counts, staining of IFN γ or CD25 for flow cytometry. Resulting 2D2 cell counts were measured and normalized as a fold-change in comparison to myelin-specific 2D2 T cells cultured alone (no APC) and treated with MOGp₁₋₁₂₅ (dashed line) (left graph). Data in **d** are pooled from two independent experiments and data are representative of two (**b-c**) independent experiments with similar results. Data were necessarily pooled in noted experiments due to limited cell numbers. Results are shown as mean \pm s.d. Statistics are calculated by one-way analysis of variance (ANOVA) with Sidak's multiple comparisons test. Data points indicate technical well replicates and dashed lines (**b-d**) indicate baseline cytokine production by 2D2 T cells alone from indicated tissues.



Extended Data Fig. 7 | Selective targeting of T cells and ILC3s through ROR γ t. **a**, Expression of MHCII was quantified by flow cytometry in indicated antigen-presenting cells from the cLN or CNS of indicated mice at steady state ($n = 4$ mice/group). **b-c** Representative flow cytometry gating strategy for indicated immune cell populations in the CNS (**b**) and expression of YFP in indicated cell populations and tissues (**c**) of Rorc-cre^{YFP} mice at day 15 of active

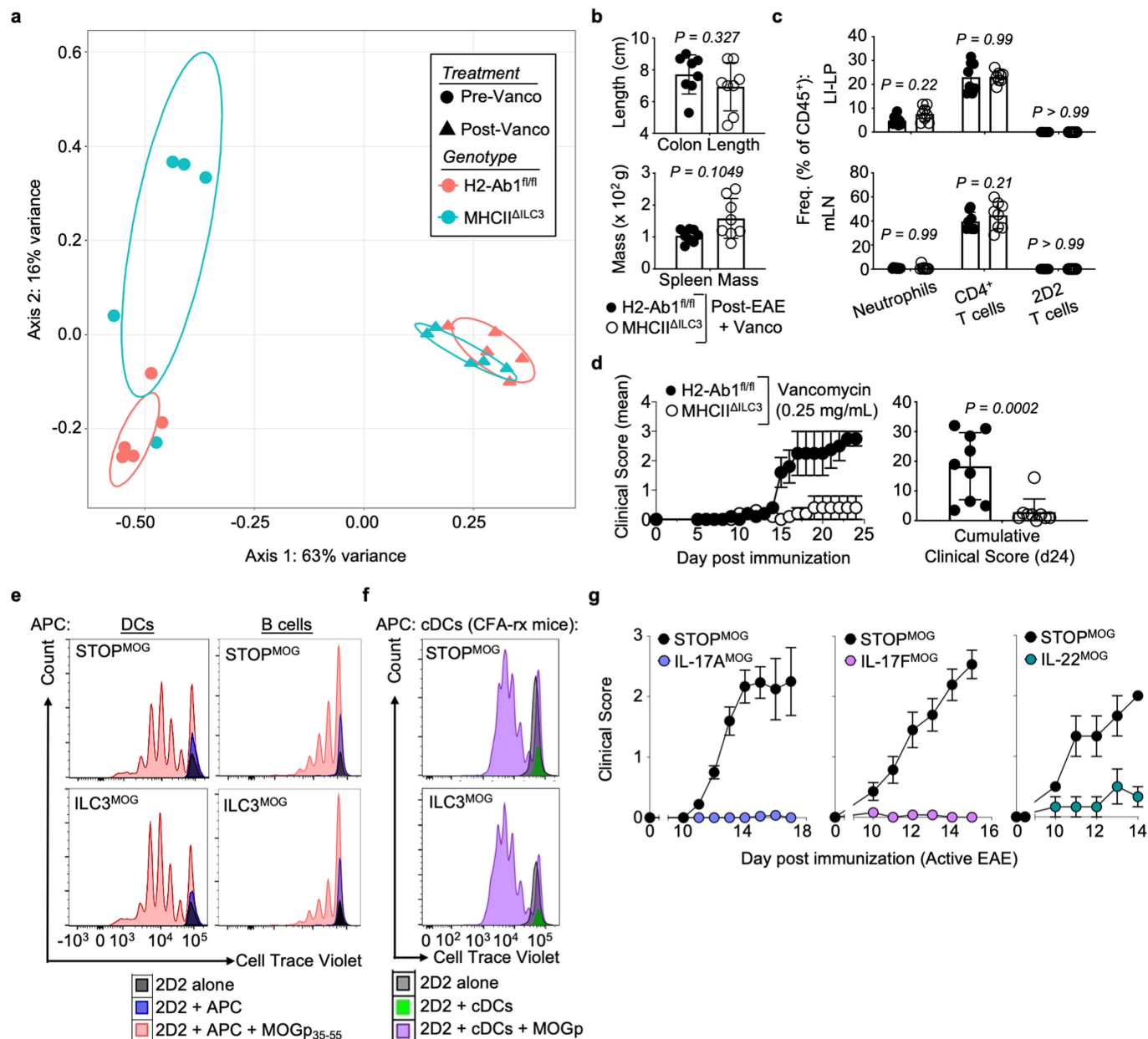
EAE. **d**, Reverse flow cytometry gating strategy defining all YFP⁺ fate-mapped cells in the CNS of Rorc-cre^{YFP} mice (day 15 EAE) (Lin 1 = B220, CD11b, CD11c, Lin 2 = CD3 ϵ , CD5, CD8, Ly6C). Results are shown as mean \pm s.d. Statistics are calculated by one-way analysis of variance (ANOVA) with Sidak's multiple comparisons test (**a**). Data in **a-d** are representative of two independent experiments with similar results.



Extended Data Fig. 8 | See next page for caption.

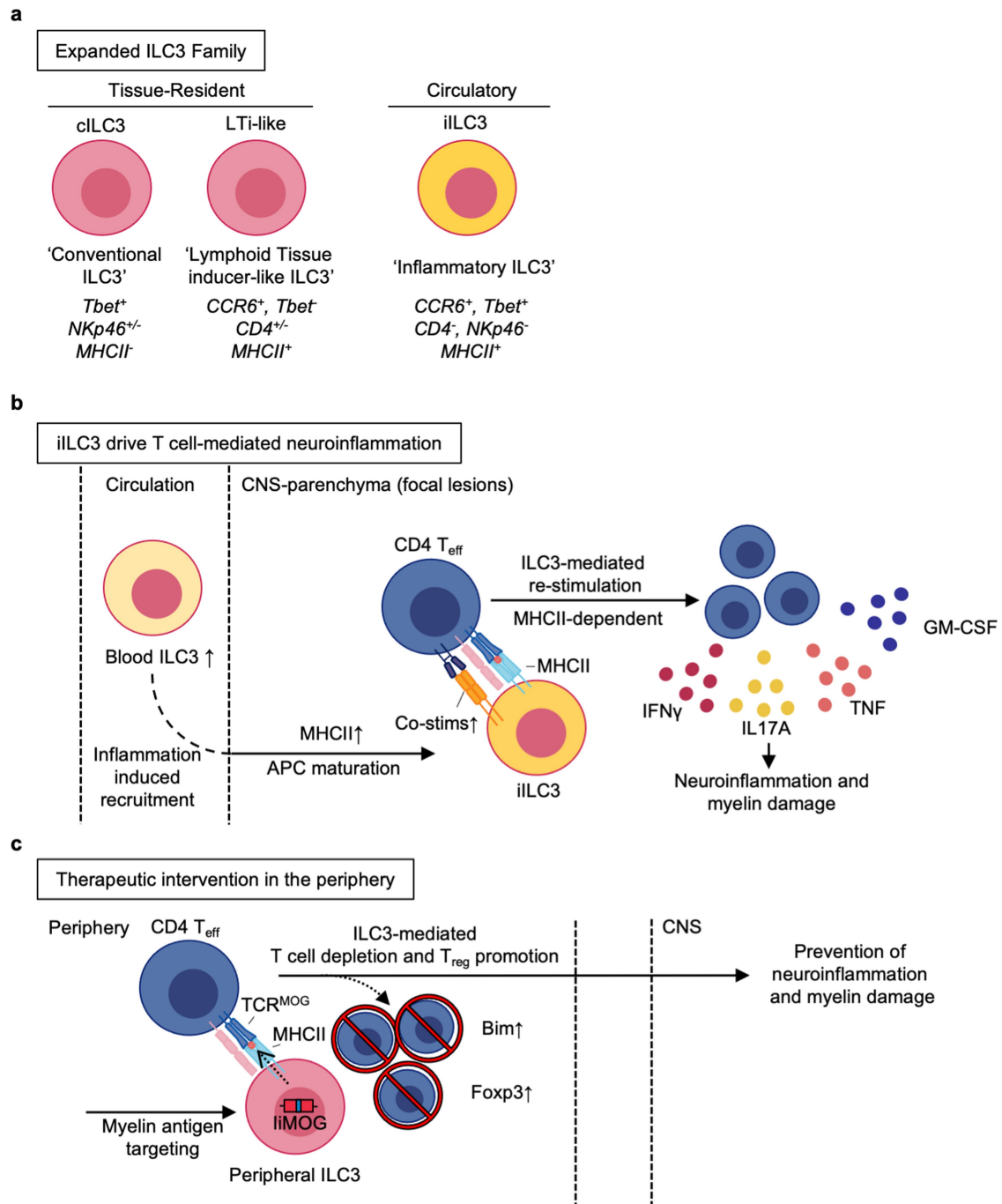
Extended Data Fig. 8 | Effect of ILC3-specific MHCII and generalized intestinal inflammation on neuroinflammation. a-d, Naive 2D2 T cells (Thy1.1⁺) were transferred into recipient mice, which were immunized 24 h later to induce active EAE. At day 14 EAE, frequencies and counts (**a**), activation/proliferation (**b**), and polarization (**c**) of donor Thy1.1⁺ 2D2 T cells (**c**, upper panel) or endogenous T cells (**c**, lower panel) were analysed by intracellular flow cytometry in the cLN or inLN (n = 9 mice/group (**a, b**), n = 5 mice/group (**c**)). **d**, Frequencies of IFN γ -producing endogenous T cells in the CNS were quantified by intracellular flow cytometry cytokine staining (n = 8 mice/group). **e-f**, Passive EAE was induced in recipient mice and day 15 frequencies of Thy1.1⁺ 2D2 T cells in the cLN and CNS were determined by flow cytometry (n = 4 mice/group) (**e**). Representative H&E of fixed transverse spinal cord sections of mice shown at 4X magnification (top, scale bar = 300 μ M) with 20X inset magnification

(bottom, scale bar = 75 μ m) of cellular infiltration near ventromedial fissure at day 15 passive EAE (**f**). **g-h**, Average clinical scores in indicated mice (MHCII ^{Δ Tcell} = CD4-cre⁺ x H2-Ab1^{fl/fl}) after induction of active EAE (n = 4 mice/group (**g**), n = 5 mice/group (**h**)). **i**, C57BL/6 mice were treated with either 3% D.S.S. in the drinking water for 7 days or were orally gavaged with *C. rodentium* (n = 5 mice/group). Active EAE was induced 14 days later and clinical scores were taken on mice or controls. Data are representative of two (**g-i**) or three (**a-f**) independent experiments with similar results. Data are pooled from two independent experiments in **a, b, d**. Results are shown as mean \pm s.d. (**a-e**) or s.e.m (**g-i**) Statistics are calculated by two-way analysis of variance (ANOVA) (**c, d**) with Sidak's multiple comparisons test or unpaired, two-tailed *t*-test (Mann-Whitney U-test) (**a, b, e**).



Extended Data Fig. 9 | Targeting peripheral ILC3s and their role in neuroinflammation. **a-d**, Littermate H2-Ab1^{fl/fl} and MHCII^{ΔILC3} mice were treated with Vancomycin (Vanco) in the drinking water for 7 days prior to induction of active EAE and Vanco was continued throughout EAE. **a**, PCoA (Weighted UniFrac) of 16S rRNA gene sequencing of faecal samples at indicated treatment timepoints (n = 5 mice/group, rep. of N = 2). At the end of EAE plus vancomycin treatment, **b**, colon lengths, spleen mass, **c**, and total frequencies of endogenous neutrophils, CD4⁺ T cells, and transferred Thy1.1+ 2D2 T cells in the indicated gastro-intestinal tissues. LI-LP = large intestine lamina propria. **d**, Daily (n = 5 mice/group) and cumulative clinical scores of mice (n = 9 mice/group, pooled from N = 2). **e-f**, Splenic antigen-presenting cells (APCs: DCs or B cells) were sort-purified from steady state (**e**) or CFA-treated mice (**f**, d10) and co-cultured with 2D2 T cells previously stained with violet cell trace violet.

Groups included 2D2 T cells alone (no APC), 2D2 T cells plus APC, or 2D2 T cells plus APC and MOG peptide. After 72 h, proliferation of 2D2 T cells was determined by flow cytometry to measure cell trace violet dilution from cell division. **g**, Average clinical scores in indicated mice after induction of active EAE (n = 18-21 mice/group left panel pooled from three independent experiments with similar results, n = 13-4 mice/group middle panel pooled from three independent experiments with similar results, right panel n = 3 mice/group representative of two independent experiments with similar results). Results are shown as mean \pm s.e.m. (**d** left panel, **g**) or mean \pm s.d. (**a-c**, **d** right panel). Statistics are calculated by two-tailed t-test (Mann-Whitney U-test) (**b**, **d**) or two-way analysis of variance (ANOVA) (**c**) with Sidak's multiple comparisons test. Results in **a** are representative of two independent experiments (n = 4-5 mice/group) and data in **b-d** are pooled from N = 2.



Extended Data Fig. 10 | Antigen presenting group 3 innate lymphoid cells orchestrate neuroinflammation. **a**, ILC3 family heterogeneity with inflammatory ILC3s (iILC3s) depicted in yellow. **b**, During autoimmune neuroinflammation, iILC3s enter the CNS from the circulation and are essential

to promote pro-inflammatory T cell responses and demyelinating disease through antigen presentation. **c**, Tissue-resident and peripheral ILC3s retain tolerogenic potential, and when targeted to express myelin peptide can eliminate self-specific T cells and prevent demyelinating disease.

Reporting Summary

Nature Portfolio wishes to improve the reproducibility of the work that we publish. This form provides structure for consistency and transparency in reporting. For further information on Nature Portfolio policies, see our [Editorial Policies](#) and the [Editorial Policy Checklist](#).

Statistics

For all statistical analyses, confirm that the following items are present in the figure legend, table legend, main text, or Methods section.

n/a Confirmed

- The exact sample size (n) for each experimental group/condition, given as a discrete number and unit of measurement
- A statement on whether measurements were taken from distinct samples or whether the same sample was measured repeatedly
- The statistical test(s) used AND whether they are one- or two-sided
Only common tests should be described solely by name; describe more complex techniques in the Methods section.
- A description of all covariates tested
- A description of any assumptions or corrections, such as tests of normality and adjustment for multiple comparisons
- A full description of the statistical parameters including central tendency (e.g. means) or other basic estimates (e.g. regression coefficient) AND variation (e.g. standard deviation) or associated estimates of uncertainty (e.g. confidence intervals)
- For null hypothesis testing, the test statistic (e.g. F , t , r) with confidence intervals, effect sizes, degrees of freedom and P value noted
Give P values as exact values whenever suitable.
- For Bayesian analysis, information on the choice of priors and Markov chain Monte Carlo settings
- For hierarchical and complex designs, identification of the appropriate level for tests and full reporting of outcomes
- Estimates of effect sizes (e.g. Cohen's d , Pearson's r), indicating how they were calculated

Our web collection on [statistics for biologists](#) contains articles on many of the points above.

Software and code

Policy information about [availability of computer code](#)

Data collection

All flow cytometry experiments were performed using a LSR Fortessa flow cytometer and the FACS Diva software (BD Biosciences) and analyzed with FlowJo v.10 software (Tree Star, Inc.) or sort-purified by using FACSAria II cell sorter (BD Biosciences). RNA-sequencing was performed on an Illumina HiSeq 4000, Raw sequencing reads were demultiplexed with Illumina CASAVA (v.1.8.2). Adapters were trimmed from reads using FLEXBAR (v.2.4) and reads were aligned to the NCBI GRCm38/mm10 mouse genome using the STAR aligner (v.2.3.0) with default settings. Reads per gene were counted using Rsubread. DNA from 16S sequencing was quantified using Quant-iT dsDNA High Sensitivity Assay Kit using Promega GloMax plate reader on a microplate (655087). Amplicon libraries were washed using Beckman Coulter AMPure XP magnetic beads. Library quality and size verification was performed using a PerkinElmer LabChip GXII instrument with DNA 1K Reagent Kit (CLS760673). Library concentrations were quantified using Quant-iT dsDNA High Sensitivity Assay Kit using Promega GloMax plate reader on a microplate (655087). No other unique software or code was used for data collection.

Data analysis

Flow Cytometry data analyzed by FlowJo V10, Statistical analysis all conducted using GraphPad Prism (v.9.2.0). RNA-sequencing Differential expression was assessed using DESeq2 version 1.14.0 with default parameters and with a false discovery rate (FDR) of 0.1. Principal component analysis was performed after using DESeq2 variance stabilizing transformation. Heat maps of the normalized gene counts, represented either as $\log_2(1 + x)$ or Z-score, were generated using Morpheus (<https://software.broadinstitute.org/morpheus>). For 16S seq Libraries were normalized to 2nM using the PerkinElmer Zephyr G3 NGS Workstation (133750) and pooled together using the same volume across all normalized libraries into a 1.5ml Eppendorf DNA tube (022431021). Pooled libraries were sequenced on the Illumina MiSeq instrument at loading concentration of 8pM with 10% PhiX, paired-end 250 using MiSeq Reagent Kit v2, 500-cycles (MS-102-2003). Demultiplexed raw reads were processed to generate an operational taxonomic unit (OTU) table using USEARCH version 11.0.667 (Edgar, 2010)63. Forward and reverse reads were merged using a maximum of 5 mismatches in the overlap region, a minimum sequence identity in the overlap region of 90 percent, a minimum overlap length of 16 base pairs, and a minimum merged sequence length of 300 base pairs. PhiX contamination was then removed, followed by quality filtering based on FASTQ quality scores, with a maximum expected error number of 1.0. OTU clustering was performed using usearch -cluster_otus with default settings. Merged (pre-filter) reads were mapped to the OTU sequences to generate the OTU table. Taxonomic classification of OTU representative sequences was performed using usearch -sintax, an implementation of the SINTAX algorithm (Edgar, 2016, pre-print: <http://dx.doi.org/10.1101/074161>), using version 16 of the Ribosomal

Database Project (RDP) Training Set (Cole et al., 2014)⁶⁴. Alpha diversity estimation and principal coordinate analysis (PCoA) were performed using the phyloseq R package (McMurdie and Holmes, 2013)⁶⁵. A phylogenetic tree was generated from the OTU representative sequences using usearch -cluster_aggd with default settings.

For manuscripts utilizing custom algorithms or software that are central to the research but not yet described in published literature, software must be made available to editors and reviewers. We strongly encourage code deposition in a community repository (e.g. GitHub). See the Nature Portfolio [guidelines for submitting code & software](#) for further information.

Data

Policy information about [availability of data](#)

All manuscripts must include a [data availability statement](#). This statement should provide the following information, where applicable:

- Accession codes, unique identifiers, or web links for publicly available datasets
- A description of any restrictions on data availability
- For clinical datasets or third party data, please ensure that the statement adheres to our [policy](#)

ILC3 RNA sequencing data are available at Gene Expression Omnibus under accession number GSE165580 and the fecal 16S data are deposited on NCBI SRA with BioProject accession number PRJNA761714.

Field-specific reporting

Please select the one below that is the best fit for your research. If you are not sure, read the appropriate sections before making your selection.

- Life sciences Behavioural & social sciences Ecological, evolutionary & environmental sciences

For a reference copy of the document with all sections, see [nature.com/documents/nr-reporting-summary-flat.pdf](https://www.nature.com/documents/nr-reporting-summary-flat.pdf)

Life sciences study design

All studies must disclose on these points even when the disclosure is negative.

Sample size	Animal sample size estimates were determined using power analysis (power=90% and alpha=0.05) based on the mean and standard deviation from our previous studies and/or pilot studies using at least 3 animals per group.
Data exclusions	Only mice experiencing clinical EAE with a score greater than or equal to 2 were utilized for sorting cells for RNA-seq. Mice with clinical score less than or equal to 1 were excluded from sorting. Otherwise, no samples were excluded from analysis.
Replication	All attempts at replication of experiments were successful and were performed at least two to three times unless otherwise noted.
Randomization	Animal experiments were not randomized because littermate group allocation was performed via animal genotype.
Blinding	Because animals were allocated by genotype, the investigators were not blinded to allocation during experiments and clinical assessment.

Reporting for specific materials, systems and methods

We require information from authors about some types of materials, experimental systems and methods used in many studies. Here, indicate whether each material, system or method listed is relevant to your study. If you are not sure if a list item applies to your research, read the appropriate section before selecting a response.

Materials & experimental systems

n/a	Involved in the study
<input type="checkbox"/>	<input checked="" type="checkbox"/> Antibodies
<input checked="" type="checkbox"/>	<input type="checkbox"/> Eukaryotic cell lines
<input checked="" type="checkbox"/>	<input type="checkbox"/> Palaeontology and archaeology
<input type="checkbox"/>	<input checked="" type="checkbox"/> Animals and other organisms
<input type="checkbox"/>	<input checked="" type="checkbox"/> Human research participants
<input checked="" type="checkbox"/>	<input type="checkbox"/> Clinical data
<input checked="" type="checkbox"/>	<input type="checkbox"/> Dual use research of concern

Methods

n/a	Involved in the study
<input checked="" type="checkbox"/>	<input type="checkbox"/> ChIP-seq
<input type="checkbox"/>	<input checked="" type="checkbox"/> Flow cytometry
<input checked="" type="checkbox"/>	<input type="checkbox"/> MRI-based neuroimaging

Antibodies

Antibodies used

Specific antibody clone/conjugates used are described below (Used at 1:200 dilution unless otherwise noted). Notation:
Target [clone] (dilution): (Conjugate, Company, Catalog Number, URL).

For mouse cell-surface staining:

B220 [RA3-6B2]: (PerCP Cy5.5, Biolegend, 103236, <https://www.biolegend.com/en-us/products/percp-cyanine5-5-anti-mouse-human-cd45r-b220-antibody-4267?GroupID=BLG6847>), (APC-F750, Biolegend, 103260, <https://www.biolegend.com/en-ie/products/apc-fire-750-anti-mouse-human-cd45r-b220-antibody-13003?GroupID=GROUP658>)

CCR6 [29-2L17]: (BV421, Biolegend, 129818, <https://www.biolegend.com/en-us/products/brilliant-violet-421-anti-mouse-cd196-ccr6-antibody-7137?GroupID=BLG6072>), (BV605, Biolegend, 129819, <https://www.biolegend.com/en-gb/products/brilliant-violet-605-anti-mouse-cd196-ccr6-antibody-8870?GroupID=BLG7289>)

CD11b [M1/70]: (PerCP Cy5.5, Thermo Fisher, 45-0112-82, <https://www.thermofisher.com/antibody/product/CD11b-Antibody-clone-M1-70-Monoclonal/45-0112-82>), (BV650, Biolegend, 101239, <https://www.biolegend.com/en-us/products/brilliant-violet-650-anti-mouse-human-cd11b-antibody-7638>), (APC-F750, Biolegend, 101262, <https://www.biolegend.com/en-us/search-results/apc-fire-750-anti-mouse-human-cd11b-antibody-13047>)

CD11c [N418]: (PerCP Cy5.5, Thermo Fisher, 45-0114-82, <https://www.thermofisher.com/antibody/product/CD11c-Antibody-clone-N418-Monoclonal/45-0114-82>), (PE-Cy7, Biolegend, 117318, <https://www.biolegend.com/en-us/products/pe-cyanine7-anti-mouse-cd11c-antibody-3086?GroupID=BLG11937>), (APC, Thermo Fisher, 17-0114-82, <https://www.thermofisher.com/antibody/product/CD11c-Antibody-clone-N418-Monoclonal/17-0114-82>), (APC-ef780, Thermo Fisher, 7-0114-82, <https://www.thermofisher.com/antibody/product/CD11c-Antibody-clone-N418-Monoclonal/47-0114-82>)

CD127 [A7R34]: (FITC, Thermo Fisher, 11-1271-82, <https://www.thermofisher.com/antibody/product/CD127-Antibody-clone-A7R34-Monoclonal/11-1271-82>), (BV421, Biolegend, 135024, <https://www.biolegend.com/en-us/products/brilliant-violet-421-anti-mouse-cd127-il-7ralpha-antibody-7193?GroupID=BLG7953>), (BV711, Biolegend, 135035, <https://www.biolegend.com/en-us/products/brilliant-violet-711-anti-mouse-cd127-il-7ralpha-antibody-10632?GroupID=BLG7953>), (PE-Cy7, Biolegend, 135014, <https://www.biolegend.com/en-us/products/pe-cyanine7-anti-mouse-cd127-il-7ralpha-antibody-6192?GroupID=BLG7953>)

CD172a (SIRPa) [P84]: (PE/Dazzle 594, Biolegend, 144016, <https://www.biolegend.com/de-de/search-results/pe-dazzle-594-anti-mouse-cd172a-sirpalha-antibody-10804>)

CD19 [1D3]: (PerCP Cy5.5, Thermo Fisher, 45-0193-82, <https://www.thermofisher.com/antibody/product/CD19-Antibody-clone-eBio1D3-1D3-Monoclonal/45-0193-82>), (PE-Cy7, Thermo Fisher, 25-0193-82, <https://www.thermofisher.com/antibody/product/CD19-Antibody-clone-eBio1D3-1D3-Monoclonal/25-0193-82>)

CD25 [PC61]: (BUV395, BD Bioscience, 564022, <https://www.bdbiosciences.com/en-us/products/reagents/flow-cytometry-reagents/research-reagents/single-color-antibodies-ruo/buv395-rat-anti-mouse-cd25.564022>)

CD252 (OX40L) [RM234L]: (Alexa Fluor 647, Biolegend, 108810, <https://www.biolegend.com/en-us/search-results/alexa-fluor-647-anti-mouse-cd252-ox40l-antibody-6460?GroupID=BLG9809>)

CD3 [17A2]: (BV605, Biolegend, 100237, <https://www.biolegend.com/en-us/products/brilliant-violet-605-anti-mouse-cd3-antibody-8503?GroupID=BLG6740>)

CD30L(CD153) [RM153]: (BV785, BD Bioscience, 740942, <https://www.bdbiosciences.com/en-in/products/reagents/flow-cytometry-reagents/research-reagents/single-color-antibodies-ruo/bv786-rat-anti-mouse-cd153.740942>)

CD3e [145-2C11]: (PerCP Cy5.5, Thermo Fisher, 45-0031-82, <https://www.thermofisher.com/antibody/product/CD3e-Antibody-clone-145-2C11-Monoclonal/45-0031-82>), (PE-Cy7, Biolegend, 100320, <https://www.biolegend.com/en-us/search-results/pe-cyanine7-anti-mouse-cd3epsilon-antibody-1899>), (APC, Thermo Fisher, 17-0031-82, <https://www.thermofisher.com/antibody/product/CD3e-Antibody-clone-145-2C11-Monoclonal/17-0031-82>)

CD4 [RM4-5]: (FITC, Thermo Fisher, 11-0042-85, <https://www.thermofisher.com/antibody/product/CD4-Antibody-clone-RM4-5-Monoclonal/11-0042-82>), (BV650, Biolegend, 100546, <https://www.biolegend.com/en-us/products/brilliant-violet-650-anti-mouse-cd4-antibody-7634>), [GK1.5]: (BV605, Biolegend, 100451, <https://www.biolegend.com/en-us/products/brilliant-violet-605-anti-mouse-cd4-antibody-10708?GroupID=BLG4745>), (BUV395, BD Bioscience, 563790, <https://www.bdbiosciences.com/en-us/products/reagents/flow-cytometry-reagents/research-reagents/single-color-antibodies-ruo/buv395-rat-anti-mouse-cd4.563790>)

CD40 [3/23]: (BV650, BD Bioscience, 740492, <https://www.bdbiosciences.com/en-eu/products/reagents/flow-cytometry-reagents/research-reagents/single-color-antibodies-ruo/bv650-rat-anti-mouse-cd40.740492>)

CD44 [IM7]: (APC-F750, Biolegend, 103062, <https://www.biolegend.com/en-us/products/apc-fire-750-anti-mouse-human-cd44-antibody-13231?GroupID=BLG10248>)

CD45 [30-F11]: (BV605, Biolegend, 103140, <https://www.biolegend.com/en-us/products/brilliant-violet-605-anti-mouse-cd45-antibody-8721>), (BV785, Biolegend, 103149, <https://www.biolegend.com/en-us/products/brilliant-violet-785-anti-mouse-cd45-antibody-10636?GroupID=BLG1932>)

CD45.1 [A20]: (eF450, Thermo Fisher, 48-0453-82, <https://www.thermofisher.com/antibody/product/CD45-1-Antibody-clone-A20-Monoclonal/48-0453-82>)

CD45.2 [104]: (BV605, Biolegend, 109841, <https://www.biolegend.com/fr-fr/search-results/brilliant-violet-605-anti-mouse-cd45-2-antibody-9695>)

CD5 [53-7.3]: (PerCP Cy5.5, Biolegend, 100624, <https://www.biolegend.com/en-us/products/percp-cyanine5-5-anti-mouse-cd5-antibody-9760?GroupID=BLG6762>), (PE-Cy7, Biolegend, 100622, <https://www.biolegend.com/en-us/products/pe-cyanine7-anti-mouse-cd5-antibody-9054?GroupID=BLG6762>), (APC, Biolegend, 100626, <https://www.biolegend.com/en-us/products/apc-anti>)

mouse-cd5-antibody-9923?GroupID=BLG6762)

CD62L [MEL-14]: (PE-Cy7, Thermo Fisher, 25-0621-82, <https://www.thermofisher.com/antibody/product/CD62L-L-Selectin-Antibody-clone-MEL-14-Monoclonal/25-0621-82>), (AF700, Thermo Fisher, 56-0621-82, <https://www.thermofisher.com/antibody/product/CD62L-L-Selectin-Antibody-clone-MEL-14-Monoclonal/56-0621-82>)

CD64 (FcYRI) [X54-5/7.1]: (BV421, Biolegend, 139309, <https://www.biolegend.com/en-us/search-results/brilliant-violet-421-anti-mouse-cd64-fcgmari-antibody-8992>)

CD80 [16-10A1]: (FITC, Thermo Fisher, 11-0801-85, <https://www.thermofisher.com/antibody/product/CD80-B7-1-Antibody-clone-16-10A1-Monoclonal/11-0801-82>), (PE, Biolegend, 104708, <https://www.biolegend.com/en-us/products/pe-anti-mouse-cd80-antibody-43>)

CD86 [GL1]: (BUV395, BD Bioscience, 564199, <https://www.bdbiosciences.com/en-us/products/reagents/flow-cytometry-reagents/research-reagents/single-color-antibodies-ruo/buv395-rat-anti-mouse-cd86.564199>), (PE, Thermo Fisher, 12-0862-82, <https://www.thermofisher.com/antibody/product/CD86-B7-2-Antibody-clone-GL1-Monoclonal/12-0862-82>)

CD8a [53-6.7]: (PerCP Cy5.5, Biolegend, 100734, <https://www.biolegend.com/en-us/products/percp-cyanine5-5-anti-mouse-cd8a-antibody-4255?GroupID=BLG2559>), (PE-Cy7, Biolegend, 100722, <https://www.biolegend.com/ja-jp/search-results/pe-cyanine7-anti-mouse-cd8a-antibody-1906?GroupID=BLG2559>)

CD90.1 [OX-7]: (PerCP Cy5.5, Biolegend, 202516, <https://www.biolegend.com/en-us/products/percp-cyanine5-5-anti-rat-cd90mouse-cd901-thy-11-antibody-4514?GroupID=BLG10566>), [HIS51]: (APC, Thermo Fisher, 17-0900-82, <https://www.thermofisher.com/antibody/product/CD90-1-Thy-1-1-Antibody-clone-HIS51-Monoclonal/17-0900-82>)

CD90.2 [53-2.1]: (PE, Thermo Fisher, 12-0902-83, <https://www.thermofisher.com/antibody/product/CD90-2-Thy-1-2-Antibody-clone-53-2-1-Monoclonal/12-0902-82>), [30-H12]: (AF700, Biolegend, 105320, <https://www.biolegend.com/de-at/products/alexa-fluor-700-anti-mouse-cd90-2-antibody-3412?GroupID=BLG6895>)

F4/80 [BM8]: (PE-Cy7, Thermo Fisher, 25-4801-82, <https://www.thermofisher.com/antibody/product/F4-80-Antibody-clone-BM8-Monoclonal/25-4801-82>), (AF700, Biolegend, 123130, <https://www.biolegend.com/en-us/search-results/alexa-fluor-700-anti-mouse-f4-80-antibody-6556?GroupID=BLG5319>)

KLRG1 [2F1]: (BV605, Biolegend, 138419, <https://www.biolegend.com/en-us/products/brilliant-violet-605-anti-mouse-human-klrg1-mafa-antibody-9644>)

Ly6C [HK1.4]: (PE-Cy7, Biolegend, 128018, <https://www.biolegend.com/en-us/search-results/pe-cyanine7-anti-mouse-ly-6c-antibody-6063>), (APC-ef780 Invitrogen, 47-5932-82, <https://www.thermofisher.com/antibody/product/Ly-6C-Antibody-clone-HK1-4-Monoclonal/47-5932-82>), (PerCP Cy5.5, Thermo Fisher, 45-5932-82, <https://www.thermofisher.com/antibody/product/Ly-6C-Antibody-clone-HK1-4-Monoclonal/45-5932-82>)

Ly6G [1A8]: (BUV395, BD Bioscience, 563978, <https://www.bdbiosciences.com/en-us/products/reagents/flow-cytometry-reagents/research-reagents/single-color-antibodies-ruo/buv395-rat-anti-mouse-ly-6g.563978>)

MHCI (I-A/I-E) [M5/114.15.2]: (APC, Biolegend, 107614, <https://www.biolegend.com/en-us/products/apc-anti-mouse-i-a-i-e-antibody-2488?GroupID=BLG4736>), (eF450, Thermo Fisher, 48-5321-82, <https://www.thermofisher.com/antibody/product/MHC-Class-II-I-A-I-E-Antibody-clone-M5-114-15-2-Monoclonal/48-5321-82>), [2G9]: (BUV395, BD Bioscience, 743876, <https://www.bdbiosciences.com/en-us/products/reagents/flow-cytometry-reagents/research-reagents/single-color-antibodies-ruo/buv395-rat-anti-mouse-i-a-i-e.743876>)

NK1.1 [PK136]: (PerCP Cy5.5, Thermo Fisher, 45-5941-82, <https://www.thermofisher.com/antibody/product/NK1-1-Antibody-clone-PK136-Monoclonal/45-5941-82>)

Nkp46 [29A1.4]: (PE/Dazzle 594, Biolegend, 137630, <https://www.biolegend.com/en-gb/products/pe-dazzle-594-anti-mouse-cd335-nkp46-antibody-13172>), (PE, Biolegend, 137604, <https://www.biolegend.com/en-us/products/pe-anti-mouse-cd335-nkp46-antibody-6523>)

TCRg/d [GL3]: (PerCP Cy5.5, Biolegend, 118118, <https://www.biolegend.com/en-us/search-results/percp-cyanine5-5-anti-mouse-tcr-gamma-delta-antibody-6702>)

XCR1 [ZET]: (FITC, Biolegend, 148210, <https://www.biolegend.com/en-us/search-results/fitc-anti-mouse-rat-xcr1-antibody-10398>), (BV650, Biolegend, 148220, <https://www.biolegend.com/de-de/products/brilliant-violet-650-anti-mouse-rat-xcr1-antibody-12421>)

For mouse intracellular staining:

Bim [C34C5]: (Alexa Fluor 647, Cell Signaling 10408S <https://www.cellsignal.com/products/antibody-conjugates/bim-c34c5-rabbit-mab-alexa-fluor-647-conjugate/10408>)

Foxp3 [FJK-16s]: (AF700, Thermo Fisher, 56-5773-82, <https://www.thermofisher.com/antibody/product/FOXP3-Antibody-clone-FJK-16s-Monoclonal/56-5773-82>)

GM-CSF [MP1-22E9]: (PE, Biolegend, 505406, <https://www.biolegend.com/ja-jp/products/pe-anti-mouse-gm-csf-antibody-958>)

IFN γ [XMG1.2]: (BV421, Biolegend, 505830, <https://www.biolegend.com/en-us/products/brilliant-violet-421-anti-mouse-ifn-gamma-antibody-7154?GroupID=GROUP24>)

IL-17A [17B7]: (FITC, Thermo Fisher, 11-7177-81, <https://www.thermofisher.com/antibody/product/IL-17A-Antibody-clone-eBio17B7-Monoclonal/11-7177-81>)

Ki67 [SolA15]: (FITC, Thermo Fisher, 11-5698-82, <https://www.thermofisher.com/antibody/product/Ki-67-Antibody-clone-SolA15-Monoclonal/11-5698-82>)

RORgt [B2D]: (PE, Thermo Fisher, 12-6981-82, <https://www.thermofisher.com/antibody/product/ROR-gamma-t-Antibody-clone-B2D-Monoclonal/12-6981-82>), (PE-ef610, Thermo Fisher, 61-6981-82, <https://www.thermofisher.com/antibody/product/ROR-gamma-t-Antibody-clone-B2D-Monoclonal/61-6981-82>)

T-bet [4B10]: (BV421, Biolegend, 644816, <https://www.biolegend.com/en-us/products/brilliant-violet-421-anti-t-bet-antibody-7281?GroupID=BLG6433>), (eFluor 660, Invitrogen, 50-5825-82, <https://www.thermofisher.com/antibody/product/T-bet-Antibody-clone-eBio4B10-4B10-Monoclonal/50-5825-82>)

TNFa [MP6-XT22]: (PE, Thermo Fisher, 12-7321-82, <https://www.thermofisher.com/antibody/product/TNF-alpha-Antibody-clone-MP6-XT22-Monoclonal/12-7321-82>), (APC, Invitrogen, 17-7321-81, <https://www.thermofisher.com/antibody/product/TNF-alpha-Antibody-clone-MP6-XT22-Monoclonal/17-7321-82>)

For human surface staining:

CD19 [HIB19], (FITC, Thermo Fisher, 11-0199-41, <https://www.thermofisher.com/antibody/product/CD19-Antibody-clone-HIB19-Monoclonal/11-0199-42>)

CD94 [DX22] (1:50): (FITC, Thermo Fisher, 11-0949-42, <https://www.thermofisher.com/antibody/product/CD94-Antibody-clone-DX22-Monoclonal/11-0949-42>)

CD14 [M5E2]: (FITC, Thermo Fisher, MHCD1401, <https://www.thermofisher.com/antibody/product/CD14-Antibody-clone-TuK4-Monoclonal/MHCD1401>)

CD123 [6H6]: (FITC, Thermo Fisher, 11-1239-42, <https://www.thermofisher.com/antibody/product/CD123-Antibody-clone-6H6-Monoclonal/11-1239-42>)

FcR1a (AER-37) [CRA1]: (FITC, Thermo Fisher, 11-5899-42, <https://www.thermofisher.com/antibody/product/FcR1-alpha-Antibody-clone-AER-37-CRA1-Monoclonal/11-5899-42>)

CD11c [BU15] (1:100): (FITC, Thermo Fisher, MA1-10085, <https://www.thermofisher.com/antibody/product/CD11c-Antibody-clone-BU15-Monoclonal/MA1-10085>)

HLA-DR [L243]: (PE, Thermo Fisher, 12-9952-42, <https://www.thermofisher.com/antibody/product/HLA-DR-Antibody-clone-L243-Monoclonal/12-9952-42>)

CD86 [BU63]: (PE/Dazzle-594, Biolegend, 374217, <https://www.biolegend.com/en-us/search-results/pe-dazzle-594-anti-human-cd86-antibody-18013>)

CD80 [L307.4]: (APC-H7, BD Biosciences, 561134, <https://www.bdbiosciences.com/eu/applications/research/b-cell-research/surface-markers/human/apc-h7-mouse-anti-human-cd80-l3074-also-known-as-l307/p/561134>)

cKit [104D2] (1:100): (PerCP-eFluor 710, Thermo Fisher, 46-1178-42, <https://www.thermofisher.com/antibody/product/CD117-c-Kit-Antibody-clone-104D2-Monoclonal/46-1178-42>)

CD127 [A019D5] (1:100): (PE-Cy7, Biolegend, 351320, <https://www.biolegend.com/en-us/products/pe-cyanine7-anti-human-cd127-il-7alpha-antibody-7216?GroupID=BLG9274>)

CD3 [UCHT1] (1:50): (BV650, Biolegend, 300468, <https://www.biolegend.com/en-us/search-results/brilliant-violet-650-anti-human-cd3-antibody-13475?GroupID=BLG5900>)

CD4 [SK3] (1:100): (BUV395, BD Biosciences, 563550, <https://www.bdbiosciences.com/en-us/products/reagents/flow-cytometry-reagents/research-reagents/single-color-antibodies-ruo/buv395-mouse-anti-human-cd4.563550>)

CD45 [HI30] (1:50): (BV605, Biolegend, 304042, <https://www.biolegend.com/en-us/products/brilliant-violet-605-anti-human-cd45-antibody-8521>)

CRTH2 [BM16] (1:50): (BV737, BD Biosciences, 741879, <https://www.bdbiosciences.com/en-us/products/reagents/flow-cytometry-reagents/research-reagents/single-color-antibodies-ruo/buv737-rat-anti-human-cd294-crth2.741879>)

For human intracellular staining:

RORgt [Q21-559] (1:50): (A647, BD Biosciences, 563620, <https://www.bdbiosciences.com/en-us/products/reagents/flow-cytometry-reagents/research-reagents/single-color-antibodies-ruo/alexa-fluor-647-mouse-anti-human-ror-t.563620>)

For in vitro culture:

anti-MHCII Class II (I-A/I-E) Monoclonal Antibody [M5/114.15.2], ThermoFisher, 16-5321-85, <https://www.thermofisher.com/antibody/product/MHC-Class-II-I-A-I-E-Antibody-clone-M5-114-15-2-Monoclonal/16-5321-85>

Purified NA/LE Hamster Anti-Mouse CD28 [37.51], BD Biosciences, 553294, <http://www.bdbiosciences.com/us/applications/research/t-cell-immunology/regulatory-t-cells/surface-markers/mouse/purified-nale-hamster-anti-mouse-cd28-3751/p/553294>

For IF/IHC:

Primary antibodies:

anti-GFP [ab6556] (1:200): (Abcam, 6556, <https://www.abcam.com/gfp-antibody-ab6556.html>)

anti-CD3 [17A2] (1:50): (Biolegend, 100202, <https://www.biolegend.com/en-us/products/purified-anti-mouse-cd3-antibody-48>)

anti-CD11c [N418] (1:50): (Thermo Fisher, 14-0114-82, <https://www.thermofisher.com/antibody/product/CD11c-Antibody-clone-N418-Monoclonal/14-0114-82>).

Secondary antibodies (all diluted 1:500):

anti-rabbit IgG-A488: (Invitrogen, A-11008, <https://www.thermofisher.com/antibody/product/Goat-anti-Rabbit-IgG-H-L-Cross-Adsorbed-Secondary-Antibody-Polyclonal/A-11008>)

anti-rat IgG-A555: (Invitrogen, A-21434, <https://www.thermofisher.com/antibody/product/Goat-anti-Rat-IgG-H-L-Cross-Adsorbed-Secondary-Antibody-Polyclonal/A-21434>)

anti-hamster IgG-647: (Invitrogen, A-21451, <https://www.thermofisher.com/antibody/product/Goat-anti-Hamster-IgG-H-L-Cross-Adsorbed-Secondary-Antibody-Polyclonal/A-21451>)

Validation

All antibodies are commercially available flow cytometry antibodies for staining mouse and human samples and are validated by the manufacturer (which can found via specific URLs provided above) and in previous publications.

Animals and other organisms

Policy information about [studies involving animals](#); [ARRIVE guidelines](#) recommended for reporting animal research

Laboratory animals

Wild-type (CD45.2+), CD45.1+ (Stock #: 3574), H2-Ab1f/f (Stock #: 013181)50, 2D2 TCRMOG transgenic (Stock #: 006912)51, Rosa-26-loxP-flanked STOP yellow fluorescent protein gene (eYFP) mice (Stock #: 006148)52, CD4-cre (Stock # 022071)53, Airefl/fl (Stock #: 031409)54, Il17aCre (Stock #: 016879)55 and Il22Cre (Stock #: 027524) mice56 on a C57BL/6J background were purchased from the Jackson Laboratory. RorcCre mice and Rorc-eGFP57 mice on C57BL/6 background were provided by G.E. liMOG (STOPMOG)42 and Il17fCre mice58 were provided by A.W. Rorc-CreERT2 mice were generated by A.D. and K.G. by inserting a codon-adapted CreERT2 cassette with Red/ET insertion kit (GeneBridges, Germany) into the transcriptional start site in exon 1 of the Rorc gene of RP24-141H23 BAC (<https://bacpacresources.org>). The vector was highly purified and injected into FVBxC57BL/6NF1 fertilized oocytes. Mice were crossed back onto C57BL/6N for more than 10 generations. For experiments with Rorc-CreERT2 mice, a 20 mg/mL solution of tamoxifen (Sigma Aldrich, USA) was prepared by suspension in olive oil (Sigma Aldrich, USA) at 37°C for 2 hours on a shaker. iMOG x RORCERT2 mice were injected intraperitoneally with 2 mg of tamoxifen, 2 days apart at day (-28) and (-30). All mice were bred and maintained in specific-pathogen-free facilities at Weill Cornell Medicine or University Mainz and littermates were used as controls in all experiments. Sex- and age-matched mice between 8 and 12 weeks of age were used for all experiments unless otherwise indicated. No mice were excluded from the analysis unless clearly indicated. All mouse experiments were approved by, and performed in accordance with, the Institutional Animal Care and Use Committee guidelines at Weill Cornell Medicine or in accordance with the guidelines of the Central Animal Facility Institution of Mainz and in accordance with relevant laws and guidelines with permission by the state Rhineland-Palatinate (animal experimentation applications (TVA) nos. G13-1-099 and G12-1-057).

Wild animals

No wild animals included.

Field-collected samples

No field-collected samples included.

Ethics oversight

All mouse experiments were approved by, and performed in accordance with, the Institutional Animal Care and Use Committee guidelines at Weill Cornell Medicine or in accordance with the guidelines of the Central Animal Facility Institution of Mainz and in accordance with relevant laws and guidelines with permission by the state Rhineland-Palatinate (animal experimentation applications (TVA) nos. G13-1-099 and G12-1-057).

Note that full information on the approval of the study protocol must also be provided in the manuscript.

Human research participants

Policy information about [studies involving human research participants](#)

Population characteristics

The description of research participants is reported in the methods in the "Human patient sample consents" section and more specifically described in Table 1 and Table 2.

Recruitment

All RRMS study subjects were recruited according to Weill Cornell Medicine Institutional Review Board–approved protocol #1003010940. Inclusion into the MS arm required a diagnosis of confirmed MS based on the 2010 revised McDonald criteria⁵⁶. Subjects having a 1st or 2nd degree relative with a diagnosis of MS or a clinically isolated syndrome were excluded

from the healthy control (HC) arm. Inclusion Criteria: 1. Subjects with clinically definite multiple sclerosis – male and female patients 18 years of age or older (Table 1) who met 2010 revised McDonald criteria. Subjects were required to have the ability to provide informed consent and be willing to participate in the study. 2. Healthy controls were enrolled for comparison. 3. Both MS patients and control subjects were excluded from the study if they did not have the ability to give consent or if they had dementia. No self-selection bias or other biases were present that could impact results.

Ethics oversight

Weill Cornell Medicine Institutional Review Board

Note that full information on the approval of the study protocol must also be provided in the manuscript.

Flow Cytometry

Plots

Confirm that:

- The axis labels state the marker and fluorochrome used (e.g. CD4-FITC).
- The axis scales are clearly visible. Include numbers along axes only for bottom left plot of group (a 'group' is an analysis of identical markers).
- All plots are contour plots with outliers or pseudocolor plots.
- A numerical value for number of cells or percentage (with statistics) is provided.

Methodology

Sample preparation

Sample preparation is described in methods in the "Isolation of cells from the blood, lymph nodes, dura meninges, CNS, and intestinal lamina propria of mice" section.

Instrument

Fortessa II and Aria II (BD Biosciences)

Software

Flow cytometry data were collected via Diva (BD Biosciences) and analyzed by FlowJo V10 (TreeStar).

Cell population abundance

The purities of sorted ILC3 cells were more than 97%, cell sorter (FACS Aria II) performance assessed before each sorting run using CS&T beads as per manufacturers instructions.

Gating strategy

Based on the pattern of FSC-A/SSC-A, cells in the lymphocyte gate were used for analysis of innate lymphoid cells and T cell subsets. Singlets were gated according to the pattern of FSC-H vs. FSC-A, followed by SSC-W vs. SSC-A. Dead cells were excluded by aqua staining (Fortessa), or cytox blue (Aria). Positive populations were determined by the specific antibodies, which were distinct from negative populations.

- Tick this box to confirm that a figure exemplifying the gating strategy is provided in the Supplementary Information.